

**DEVELOPMENT OF SEMG AND ARTIFICIAL NEURAL
NETWORKS BASED POWERED ANKLE PROSTHESIS
CONTROL ALGORITHMS FOR STAIR ASCENDING AND
DESCENDING MOTIONS**

by

Ramazan Tarık Türksöy

B.S., in Mechanical Engineering, Boğaziçi University, 2019

Submitted to the Institute of Biomedical Engineering

in partial fulfillment of the requirements

for the degree of

Master of Science

in

Biomedical Engineering

Boğaziçi University

2021

ACKNOWLEDGMENTS

I would like to thank my supervisor, Prof. Dr. Can Yücesoy for his experienced guidance and insightful advices through my Master study. I am grateful for his understanding and concern. I would also like to express my appreciation to the committee for reviewing and recommendations.

I would like to thank my dearest father Kadir Türksöy, beloved mother Fatma Türksöy and my brother Doğukan Türksöy for their love and support through my entire life. They made this work possible.

ACADEMIC ETHICS AND INTEGRITY STATEMENT

I, Ramazan Tarık Türksoy, hereby certify that I am aware of the Academic Ethics and Integrity Policy issued by the Council of Higher Education (YÖK) and I fully acknowledge all the consequences due to its violation by plagiarism or any other way.

Name :

Signature:

Date:

ABSTRACT

DEVELOPMENT OF SEMG AND ARTIFICIAL NEURAL NETWORKS BASED POWERED ANKLE PROSTHESIS CONTROL ALGORITHMS FOR STAIR ASCENDING AND DESCENDING MOTIONS

Amputation is the surgical removal of a limb due to various reasons, e.g trauma. Prosthesis is a device which is a replacement for the missing part of the limb. Ankle joint can have loads of 10-13 times of the body weight during power demanding activities. Since energetically-passive prostheses cannot generate net power output, powered ones become essential for demanding tasks. Surface electromyography (sEMG) is a non-invasive method which measures neuromuscular activity. The aim of this study was to develop artificial neural network models to predict ankle moment and position using only sEMG input for control algorithms of stair ascending and descending tasks. Time delay neural network and long short-term memory were compared for this aim. Features that represent sEMG signals better were investigated. Minimizing the number of sEMG signals from lower leg muscles can make prosthesis flexible while reducing the number of sEMG sensors required can make the prosthesis economic. Correlation of 0.90 between the predicted and actual values was set as the performance threshold. Long short-term memory based algorithms achieved significantly higher performances. 0.91 and 0.93 correlations were achieved for both motion tasks' position and moment, respectively. The minimum number of sEMG sensors was 2 for moment and 3 for position estimation. The minimum number of lower leg muscles required was 1 for moment and 2 for position estimation. The results show that there are promising EMG sensor combinations for the specified targets.

Keywords: Ankle Prosthesis, Algorithm, Electromyography, Stair Climbing, Artificial Neural Networks.

ÖZET

EMG VE YAPAY SİNİR AĞLARI TABANLI AKTİF AYAK BİLEĞİ PROTEZİ MERDİVEN ÇIKMA VE İNME HAREKETLERİ İÇİN KONTROL ALGORİTMALARI GELİŞTİRİLMESİ

Travma gibi çeşitli sebeplerle meydana gelebilen amputasyon bir uzvun cerrahi olarak kesilmesi anlamına gelir. Protez, eksik olan uzvun yerine geçen bir cihazdır. Efor gerektiren görevler esnasında, ayak bileği eklemi vücut ağırlığının 10-13 katı kadar yüke maruz kalabilir. Enerji kullanımı açısından pasif olan protezler net güç çıktısı üretmedikleri için, aktif protezler efor gerektiren hareketler için gerekli hale gelmektedir. Yüzeysel elektromiyografi (EMG) nöromüsküler aktiviteyi ölçen ve invaziv olmayan bir methodur. Bu çalışma, merdiven inme ve çıkma sırasında ayak bileği pozisyonu ve momentinin kontrolü amaçlı algoritmalar için yapay sinir ağları geliştirilmesini hedefliyor. Özellik çıkarma çalışması EMG sinyallerini en iyi temsil eden özellikleri gösteriyor. Bu hedef için zaman gecikmeli yapay sinir ağı ve uzun-kısa süreli bellek yöntemleri karşılaştırıldı. Alt bacakta kullanılacak kas sayısının azaltılması protezi farklı durumlar için esnek, toplam gerekli kas sayısının azaltılması ise ekonomik hale getirir. Performans kriteri olarak tahmin edilen değerlerle gerçek değerler arasında 0.90 korelasyon katsayısı hedeflendi. Uzun-kısa süreli bellek temelli algoritmalar daha başarılı sonuçlar verdi. Merdiven inme ve çıkma görevlerinde pozisyon ve moment için sırasıyla 0.91 ve 0.93 isabetlilik elde edildi. Başarılı pozisyon tahmini için en az 3, moment tahmini için ise 2 kastan veri gerekti. Gerekli alt bacak kas sayısı pozisyon için en az 2, moment için ise 1'dir. Çalışmanın sonuçları, hedeflenen çıktılar için başarılı ve umut vadeden EMG sensör kombinasyonları olduğunu gösteriyor.

Anahtar Sözcükler: Ayak Bileği Protezi, Algoritma, Elektromiyografi, Merdiven Çıkma, Yapay Sinir Ağları.

TABLE OF CONTENTS

ACKNOWLEDGMENTS	iii
ACADEMIC ETHICS AND INTEGRITY STATEMENT	iv
ABSTRACT	v
ÖZET	vi
LIST OF FIGURES	ix
LIST OF TABLES	xi
LIST OF ABBREVIATIONS	xii
1. INTRODUCTION	1
1.1 The Control of Powered Prosthesis	2
1.2 Surface Electromyography	3
1.3 The Biomechanics of Stair Climbing	5
1.4 Artificial Neural Networks	7
1.5 Previous Works	8
1.6 The Aims	10
2. METHODS	11
2.1 Data Set	11
2.2 Data Preprocessing	13
2.3 Sliding Window Algorithm	14
2.4 Feature Extraction	16
2.5 Feature Selection	17
2.6 Muscle Combinations	21
2.7 Neural Networks	24
2.7.1 TDNN	24
2.7.2 LSTM	25
2.7.3 Hyperparameter Optimization	26
2.7.4 The Comparison of TDNN and LSTM	28
2.8 Five-Fold Cross Validation	29
2.9 Performance Evaluation	29
3. RESULTS	31

3.1	The Comparison of TDNN and LSTM	31
3.2	Stair Ascending	32
3.2.1	Position Estimation	32
3.2.2	Moment Estimation	33
3.3	Stair Descending	34
3.3.1	Position Estimation	34
3.3.2	Moment Estimation	35
3.4	Best-Performing Variations	36
4.	DISCUSSION AND CONCLUSION	39
4.1	Future Works	42
	APPENDIX A. FEATURE EXTRACTION	44
A.1	Feature Definitions	44
A.2	Feature Performances	45
	APPENDIX B. DETAILED TEST RESULTS FOR EACH OUTPUT	47
B.1	Stair Ascending Position	47
B.2	Stair Ascending Moment	49
B.3	Stair Descending Position	52
B.4	Stair Descending Moment	55
	REFERENCES	58

LIST OF FIGURES

Figure 1.1	The periods of the stance and swing phases [1].	6
Figure 2.1	Experimental setup used for stair climbing tasks in Lencioni et al. Adapt. from [2].	12
Figure 2.2	The distribution of the number of samples per subject.	12
Figure 2.3	Comparative results of the feature sets with different sizes.	18
Figure 2.4	Intra-feature correlation analysis results for stair ascending. The darker the color the higher the correlation.	19
Figure 2.5	Intra-feature correlation analysis results for stair descending. The darker the color the higher the correlation.	19
Figure 2.6	Intra-muscle correlation analysis results for stair ascending.	22
Figure 2.7	Intra-muscle correlation analysis results for stair descending.	23
Figure 2.8	An illustration of TDNN structure. Generated via Matlab.	25
Figure 2.9	An illustration of an LSTM block showing the flow of data through gates.	25
Figure 2.10	The structure of the proposed LSTM network.	28
Figure 3.1	Box plot of stair ascending position prediction results of input sets with different number of muscles for comparison of a) TDNN, b) LSTM.	31
Figure 3.2	Box plot of stair ascending moment prediction results of input sets with different number of muscles for comparison of a) TDNN, b) LSTM.	32
Figure 3.3	Box plot of position prediction results of input sets with different number of muscles for stair ascending.	33
Figure 3.4	Box plot of moment prediction results of input sets with different number of muscles for stair ascending.	34
Figure 3.5	Box plot of position prediction results of input sets with different number of muscles for stair descending.	34
Figure 3.6	Box plot of moment prediction results of input sets with different number of muscles for stair descending.	35

Figure 3.7	Stair ascending predictions vs actual values of the best-performing muscle combination.	38
Figure 3.8	Stair descending predictions vs actual values of the best-performing muscle combination.	38

LIST OF TABLES

Table 3.1	The 15 best position prediction results. Stair ascending on the left, stair descending on the right.	36
Table 3.2	The 15 best moment prediction results. Stair ascending on the left, stair descending on the right.	37
Table A.1	The equations for some common time-domain features investigated in this study.	44
A.2	The results of feature selection study.	45
B.1	Stair ascending position estimation results with accuracy greater than 0.89.	47
B.2	Stair ascending moment estimation results, the 100 best-performing input set.	49
B.3	Stair descending position estimation results with accuracy greater than 0.89.	52
B.4	Stair descending moment estimation results, the 100 best-performing input set.	55

LIST OF ABBREVIATIONS

EMG	Electromyography
sEMG	Surface Electromyography
WA	Weight Acceptance
PU	Pull-Up
FCo	Forward Continuance
FC	Foot Clearance
FP	Foot Placement
PO	Push-Off
VM	Vastus Medialis
GM	Gluteus Maximum
BF	Biceps Femoris
RF	Rectus Femoris
TA	Tibialis Anterior
ANN	Artificial Neural Network
SOL	Soleus
MG	Gastrocnemius Medialis
PL	Peroneus Longus
FFT	Fast Fourier Transform
TDNN	Time Delay Neural Network
SSC	Slope Sign Changes
MAV	Mean Absolute Value
ZC	Zero Crossings
MAVS	Mean Absolute Value Slope
WL	Waveform Length
WAMP	Willison's Amplitude
MMAV1	Modified Mean Absolute Value
IEMG	Integrated EMG
RMS	Root Mean Square

VAR	Variance
LSTM	Long Short-Term Memory

1. INTRODUCTION

Ankle joint carries the weight of the human body, the load and the impact is even greater than walking or standing in common daily activities such as jumping and running. The load of the movement on the ankle can reach up to 10-13 times of the body weight locally during running [3]. Amputation of a part of the lower leg including the ankle because of any accidental reason or nervous system injuries such as spinal cord injury and brain injury affects human life significantly [4]. Ischemia, gangrene, infection, trauma and tumor are most common reasons for transtibial amputations [5].

Over 150000 people undergo lower limb amputation in the U.S. each year [6]. It is predicted that there will be 1.5 millions of people with major lower extremity amputations in the U.S. by 2050 [7]. According to the survey of Reiber et al., 23% of 105309 lower limb amputations are transtibial among toe, foot or ankle, hip or pelvis and transfemoral levels [8].

Along with the technological development, enhancement of assistive devices for amputees can improve their health and life quality. Prosthesis is a device which is a replacement for the missing part of the body. The aim is to assist people with amputation by taking the responsibilities of the absent limb.

According to the research of Schaffalitzky et al., lower limb prosthesis can provide an easier use especially in a home environment compared to a wheelchair. The physiological benefits of the functional independence of prosthesis are another overcome that bring self-confidence and self-sufficiency. Sense of balance and an overall improved life quality can be counted as the benefits that are observed in lower limb prosthesis users [9].

There are passive, semi-active and active or powered prostheses. Passive prostheses can absorb or store energy, but do not supply net power to the locomotion.

Since there can be a lack of power for demanding tasks, e.g., climbing stairs, standing up from sitting position, in passive and semi- active prostheses, they can be insufficient for covering daily life activities [10]. Without the net power contribution, there is an increase in metabolic energy consumption up to 30% in overall leg amputees and about 60% in transfemoral amputees. [11, 12]. Additionally, the required power of the hip joint increases over two times and the resultant gait can be more asymmetric [13, 14]. The limited services passive prostheses provide do not include variable parameters such as walking speed and different terrain types. Powered prostheses have the advantage of changing these functional variables using its ability to introduce external power through actuators. Therefore, it has the highest complexity among other types of prostheses.

The human body is a complex biomechanical system. Therefore, designing an artificial substitute for some part of the human body is difficult. Passive prostheses are more commercially available for transtibial amputations. Even though there are several products in the market, powered prosthesis has not gone commercial enough [15, 16]. There were not any commercially available powered ankle-foot prosthesis until the early 2000s [17]. The studies leading to products have been performed in the last decade [11, 18]. However, they have not utilized a generalized application for different terrains yet [11].

1.1 The Control of Powered Prosthesis

To talk about the structure of prosthesis briefly, there are sensory system to feed the control system, control system and actuation system. Sensory input can be kinetic, kinematic and/or EMG signals. Common kinetic sensors used in lower extremity prosthesis control measure ground reaction forces and moments in different directions. [19, 20]. Kinematics sensors include angle, velocity and acceleration of different joints in different directions. [21] - [22].

The design of the control system of a powered prosthesis can determine the efficiency, capability, energy consumption and the accuracy of the device. The control system has an essential role to unlock the potential of the interaction between the user and the mechanical system.

The application areas of prostheses and exoskeleton robots are unrestricted environments. There is not a common effective methodology in the prediction of human joint moments in unrestricted environments yet [23]. A reasonable way to achieve such a control strategy can be a stepwise progression by investigating different scenarios of the use of ankle prosthesis. This study can be considered as a step in this progression. Finally, a well-structured combination of them would yield an enhanced controller.

Although there are studies to develop prosthesis controllers which provide use in unconstrained grounds or adjustments to variances in the content of tasks such as changes in the carried load, there is not a commercially available one yet [24] - [25]. According to Dhir, the current controllers for powered prostheses were not able to provide generalized solutions for the variances on walking speed [26]. Current controller structures are limited with subject-specific adjustments for moment estimations at certain walking speeds [27]. This is an undesired condition for engineering applications.

1.2 Surface Electromyography

Surface electromyography (sEMG) is a common technology used for many purposes such as rehabilitation and diagnosis of neuromuscular diseases or other dysfunctions in clinical applications. In the last decade, researchers focused on the use of EMG to control lower extremity prostheses for environment and task adaptations [28]. It measures myoelectric signals from muscles which is a quantitative indicator of muscular activity. While the duration of the EMG changes with the duration of the activation of the muscle, the amount of the electrical activity produced in the muscle determines the amplitude of myoelectric signal. There are many components that affect EMG signals. Some of them are physiological characteristics of the muscle,

intramuscular coordinations and the instrumentation of signal acquisition [29].

EMG electrodes are mounted on the surface of the skin. Acquired EMG signal is a function of the whole muscle fibres' action potentials under the skin. The instant potential differences can be either positive or negative. Therefore, the amplitude of the EMG signal is more considerable than the sign [30].

sEMG is a non-invasive technique unlike needle EMG whose electrode is inserted directly into the muscle. Although needle EMG can be preferred over sEMG in steady clinical applications despite its invasiveness, it would not be comfortable for dynamic applications such as prosthetics. The ability to avoid neighbouring muscle cross-talk and getting information from a single motor unit may be the reason for preference of needle EMG over sEMG especially for clinical neurophysiological applications [31, 32].

Human joint moment is a function of the motor units' action potentials. There is a transmission time of neuromuscular signal to the muscles and leading to movement of the joints and limbs. This transmission time causes a delay of muscle and joint movements with respect to sEMG signals between 30-150 ms [33]. It is an advantage of using EMG signals in real time applications.

Collecting myoelectric signals from the muscles located in the sound parts of the leg has the general difficulties of sEMG sensors. However, the neuromuscular information gathered from the residual muscles brings additional challenges depending on the muscle-nerve attachment configuration. The quality of EMG signals is determined by many factors such as the length of the residual limb, the reason for the amputation and the technique of the surgery [34] - [35]. Although it is shown that an ankle-foot prosthesis controlled using EMG signals from the lower leg of a transtibial amputee can be used by an amputee, the possible declines in the quality of EMG signals from the residual muscles should be considered [36].

1.3 The Biomechanics of Stair Climbing

Stairs are a common terrain type in daily life. Compared to level walking, stair climbing is a power demanding locomotion task and it requires more mobility. Therefore, it could be decisive in the design of a lower limb prosthesis. Due to the rhythmic nature of stair ambulation, it has the main gait cycle concept similar to level walking. However, the properties of the gait cycle differ significantly. Thus, stair climbing can be expressed by a different phase division.

A gait cycle of a leg can be divided into two phases as stance and swing phase. Stance phase represents the duration in which the limb carries the weight of the body while it is in contact with the ground. In the swing phase, the foot is off the ground which is just the opposite of the stance phase.

Stance phase starts with the initial contact of the foot with the ground and finishes when this connection ends. The stance phase takes significantly longer time in stair ascent than level walking [37]. The stance phase of stair ascent can be divided into three periods. As soon as the initial contact occurs, the center of mass of the body shifts called weight acceptance (WA). This shift prepares a suitable position for pull-up (PU). Then, the leg fully extends and forward continuance (FCo) period occurs. When the stance phase finishes, the leg breaks contact with the stair in foot clearance (FC) period. Finally, this specified leg makes the initial contact with the next step which is called foot placement (FP). There are four periods in the swing phase with an additional period called push-off (PO). After WA, the swing phase ends with PO in which the leg is pushed off from the previous step of the stair [1]. This process is illustrated in Figure 1.1.

There is a general consideration of transition time between phases which corresponds to the 60% of a gait cycle, approximately [38, 39]. This transition in stair descent is observed close to the level walking. On the other hand, the stair ascent transition occurred slightly differently from the other locomotion tasks as stance phase lasts about 66% of the whole cycle [40].

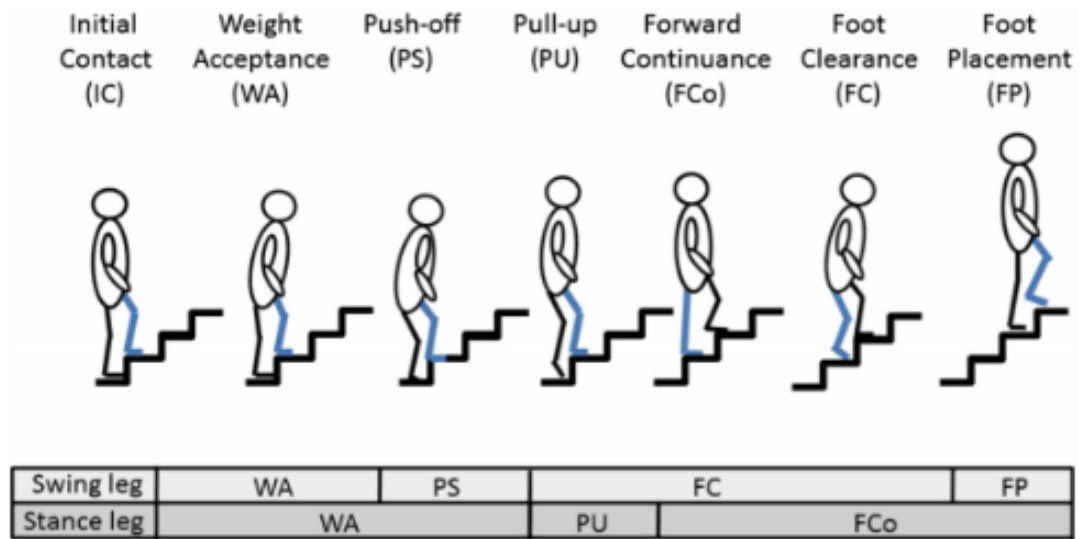


Figure 1.1 The periods of the stance and swing phases [1].

There are several factors that affect the biomechanics of stair ambulation. One of them is age. According to Marshall et al., quadriceps muscle activity was 3-times greater in older adults compared to the younger ones [41]. In the study of Farrag El-sayed, children had significantly higher muscle activation and joint angles during stair ascending and descending. Gender may also be effective in the lower limb biomechanics of stair climbing. It was observed that the joint angles of females were higher than the males' while stair climbing [42]. Besides physical differences such as height, neuromuscular and metabolic development of muscles may be effective in this variance [41] - [43].

Another factor is the locomotion speed. The changes in the speed significantly affected activation of some muscles in a study of Lewis et al [44]. For instance, increasing the speed from slow to self-selected increased the activation levels of vastus medialis (VM), gluteus maximus (GM) and biceps femoris (BF) during stair ascending and VM and rectus femoris (RF) in stair descending.

Besides the unique differences between humans, gait characteristics of stair climbing can vary with the environmental factors such as the dimensions of the steps. In the study of Riener et al., the observed transition moments were delayed as the inclination increased for stair ascending [45]. Additionally, the lower limb joint power generation during stair climbing is significantly related to the slope of the stairs [46].

The form of the stairs can also affect the joint biomechanics. According to the observations of Chang et al. on regular stairs and stairmill, maximum plantarflexion of the ankle increased and tibialis anterior (TA) activation decreased on stairmill [47].

The aforementioned factors are challenges of controller design for powered prosthesis. To make the controller more useful, the need for a generalized solution is obvious. This is one of the main focuses of the methodology of this study which is detailed in the Methods section.

1.4 Artificial Neural Networks

There are various approaches in controller design for lower limb prosthesis and assistive exoskeletons. Some of them are statistical methods such as linear discriminant analysis and Gaussian mixture models [48], neuromuscular models such as Hill-type muscle model [49, 50] and artificial neural networks (ANNs) [25, 36].

Artificial neural networks (ANNs) are already useful and also promising tools for human joint behavior prediction which includes complex mathematical biomechanics [51]. They are often referred as black box that solves but one cannot see what is inside. It simply maps the inputs to outputs. There are artificial neurons which are building blocks of the neural networks. They function as mathematical processing units taking their inputs which are the outputs of the previous neurons in the neural network structure. Another structural element is layers which are formed by neurons and they are connected to each other. ANNs learn the relationship between input and output by training. Training process occurs over many iterations. Some parameters within the

neural network, i.e. weight and bias variables, are updated with each iteration. These parameters are used in the activation functions of the neurons and they determine the outputs of each neuron together.

There is supervised, unsupervised and reinforcement learning. In supervised learning, the network is fed by labeled data. The two main types of problems being solved using supervised learning are classification and regression. The determination of which locomotion task is performed would be a classification problem. The estimation of the moment and position values is a regression problem.

1.5 Previous Works

Before continuing with Methods, the previous works on similar objectives can be reviewed to make related methodologies and performances more clear. In a recent study, for ankle torque prediction during level walking at self-selected speed a performance of RMSE=0.08 Nm was reached with an ANN model [52]. In another study of Xie et al., using general regression neural network, RMSE of 3.84 degrees is achieved for ankle angle estimation taking angle, sEMG and pressure data as sensory input. RMSE was 21.69 when only sEMG from the upper leg was used as input [53].

Manal et al. used Hill-type muscle model for ankle moment prediction with RMSE = 4.4 Nm. Sensory data was collected from TA, soleus (SOL), gastrocnemius medialis (MG) and lateral gastrocnemius of the lower leg [54]. Slajpah et al. developed an extended Kalman filter model using 7 inertial and magnetic measurement units of lower extremity and trunk. They achieved an average of 0.80-0.83 correlation between the real values and the predicted ones where the cases with the best results were slow walking with correlations of 0.86-0.89. On the other hand, this is greater than 0.90 for knee angle and higher than 0.95 for hip [55].

Most of the studies on the modelling of ankle joint behavior use sensory information from lower leg muscles or knee joint. Gastrocnemius, SOL and TA were used

in Au et al., 2005 [56]. BF, VL, MG and SE are used in Zhu et al [57] with thigh and shank angles. GM, TA, peroneus longus (PL) in Su et al [33]. SOL, TA, GM in Zhang et al [52]. External gastrocnemius, gastrocnemius, soleus, tibialis anterior and tibialis longus in Huihui et al [58].

The results and model information so far have been for level walking. As for stair climbing, the results and sensory inputs would change. At first, there are less studies on stair climbing than level walking. Because level walking is seen as the basis for prosthesis or assistive device studies, it is common to start with this type of locomotion [59]. Considering the daily role of stair ambulation and its demanding nature, this locomotion task should not be skipped for further developments of powered prosthetic and assistive devices. For instance, in the work of Weigand et al., ANN performance for gait phase estimation is lower for stair ascending and descending than level walking [60].

Au et al., 2008 used TA, MG and lateral gastrocnemius for an ankle-foot prosthesis for level walking and stair descending tasks [36]. In another study, stair descending results were the lowest with a mean accuracy of 83.5% for ankle torque among other locomotion tasks including level walking and slope walking for an ankle exoskeleton controller. Additionally, stair ascending was the second lowest one [61]. Gupta et al. developed a neural network for ankle angle estimation using sEMG signals from 6 lower limb muscles and knee angle as input. They have the following results: Average RMSE=3.61 degrees for stair ascent and average RMSE=5.04 degrees for stair descent [62].

The work of Keles and Yucesoy is a beginning for the further studies on prostheses in the Biomechanics Lab of the Biomedical Engineering Institute of Bogazici University [63]. This thesis is a part of this studies on prostheses. The work of Keles and Yucesoy was on predicting moment and position of ankle joint during level walking. The focus of the two works may seem similar. However, there are many differences which are mentioned in the later chapters.

1.6 The Aims

Considering the lack of ankle joint controllers for stair climbing task, the goal of this study was to develop sEMG-based neural network models which predict the ankle position and moment during stair ascending and descending. These models were planned to be the building blocks of the control system of powered ankle prosthesis.

To represent the EMG signals more efficiently, it was preferable to extract some statistical features of the signal. EMG feature extraction is a subject of research itself. The first specific aim was to find the best feature set which represents the EMG signals used in this study.

The comparison of neural network architectures for specific problems is also a research topic itself. To develop a more optimal model, two appropriate neural network architectures for the problem statement were studied. The second specific aim was to compare the predictive success of Time delay neural network (TDNN) and long short-term memory (LSTM).

This study seeks for the relationship between lower limb muscles and ankle moment and position during stair climbing tasks. The third specific aim was to identify the sEMG sensor requirements in terms of both the number of sensors and the number of lower leg muscles. Minimizing the number of overall EMG sensors would yield a system with lower cost, this can be called as economic solution. Due to possible surgical problems of transtibial amputation process, minimizing the number of lower leg muscles would allow a more flexible solution.

2. METHODS

2.1 Data Set

An open access data of Lencioni et al. [2] is used in this study. There are 50 healthy subjects including 25 females and 25 males. The age interval is 6-72. Body mass and heights of the subjects vary between 18.2-110 kg and 116.6-187.5 cm, respectively. The number of samples and the age range, consecutively other body characteristics, are wide compared with the studies on regression or classification tasks on human joints, especially on lower limb prediction [64]-[22]. Although there are studies using data which consists of more than 20 subjects, their age ranges are narrower [65]. Even if there is not any certain measure found to statistically obtain the following argument, it can be assumed that this data presents a higher variance based on the aforementioned data properties. Hence this study can show a noteworthy generalization ability in learning the essence of the movement form of the tasks regardless of who is performing it. Consequently, this is advantageous for real world engineering applications of the algorithm.

The devices used in data collection are a 9-camera motion capture system (SMART system, BTS, Garbagnate Milanese, Italy), two force platforms (Kistler, Winterthur, Switzerland) and a 8-channels wireless EMG recording system (ZeroWirePlus, Cometa, Bareggio, Italy). The experimental setup for stair climbing recordings and EMG sensors on the leg is in Figure 2.1.

The sampling frequency for EMG recording is 800 Hz, 960 Hz or 1000 Hz, while 3D kinematics from markers were recorded at 60 Hz or 200 Hz. There was not a strict speed requirement to perform the tasks. Therefore, they were performed at each subject's self-speed. Different sampling frequencies and variances in speed yield a data set of varying lengths. This will be detailed later in the Data Preprocessing section.



Figure 2.1 Experimental setup used for stair climbing tasks in Lencioni et al. Adapt. from [2].

Considering the tasks focused on this thesis, there are 169 stair ascending task samples from a set of 43 subjects, 1-5 samples per subject. Besides, stair descending samples consist of 146 samples of 43 subjects whose subjects slightly differ from stair ascending subject set, again 1-5 samples per subject. This distribution is shown in Figure 2.2.

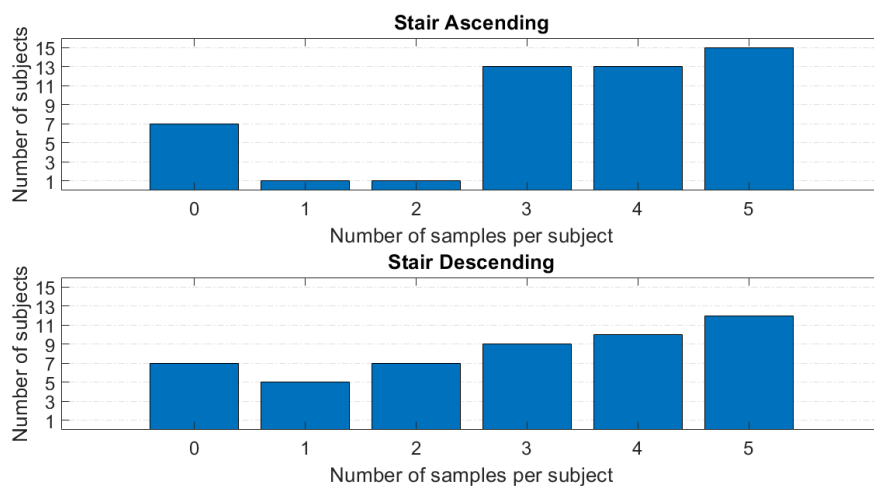


Figure 2.2 The distribution of the number of samples per subject.

Joint angles and moments were calculated from measured data. sEMG signals were filtered before sampling with a band-pass filter having cut-off frequency of 10-400 Hz. sEMG sensors were placed to measure the signals of the following muscles: tibialis anterior (TA), soleus (SOL), gastrocnemius medialis (MG), peroneus longus (PL), rectus femoris (RF), vastus medialis (VM), biceps femoris (BF) and gluteus maximus (GM).

2.2 Data Preprocessing

Signals contain noise which is not directly related with the main content. Nevertheless, it has amplitude and frequency properties which means it still is information that would probably confuse the neural network. Thus, noise is an unwanted element. Filtering is a process that allows the elimination of undesirable components from the signal. Noise can be eliminated by figuring out the frequency characteristics of it in a signal.

Neural signal decoding is not seen as sufficient. EMG cross-talk and the difficulty of acquiring clear signals are some reasons for that [66]. EMG signals can have noise because of various factors. Most of these factors are movement artifacts, skin-electrode interface, power line. Movement artifacts are indicated as low-frequency noise while skin-electrode interface equipment noise are examined as high frequency noise. Power line noise occurs at a certain frequency of 50 Hz or 60 Hz depending on the region that the electric supply is provided. Generally, high-frequency noise is considered above 400-500 Hz and low-frequency noise is below 10-20 Hz in the literature [67]-[68]

Although there are many studies on the causes of noise in EMG signals, there is not a certain property that can be applied to all muscles of the body, even for the focus of this thesis, lower limb muscles. Therefore, to understand the signal characteristics, fast Fourier transform (FFT) method is applied to the signal to identify the frequency characteristics of the data. Combining the inferences of both literature research and FFT analysis, a 4th order Butterworth band-pass filter is applied with a cut-off fre-

quency of 10 Hz - 200 Hz. Additionally, a band-stop filter with a cut-off frequency of 50 Hz is applied to avoid noise introduced by the power line. However, this did not significantly change the neural network performance. It should be noted that signal filtering process can lead to delays in EMG signal [64]. Despite the fact that noise reduces the signal quality, it is an advantage not to have to use filtering in real-time applications. Consequently, there is not any signal filtering in this study.

However, there is another signal preprocessing method that improved the results: Rectification. There are different rectification techniques. Full-wave rectification is applied to the data. Unlike half-wave rectification in which negative values become zero, all amplitudes are preserved by simply taking the absolute value of the whole signal. The reason for this preference is to keep the signal amplitudes so that the strength of the neural activity which represents the muscle activation characteristics of EMG remain [69].

For the number of data points of inputs and outputs to be equal for the neural networks, EMG data is interpolated and kinetics and kinematics data extrapolated to a certain number of data points. Increasing the number of data points would result in increased performance for time delay neural network (TDNN), while also increasing the computational cost. The number of data points of 200 is selected by a simple grid search considering both computational cost and network performance.

2.3 Sliding Window Algorithm

It is not a wise choice to use instant measurements from EMG sensors simultaneously for recognition tasks [70]. Sliding window technique which consists of a window that shifts through the data can help overcome this issue. Statistical calculations, later will be called as features, are applied to the whole data in each window. Through this process, time dependency of the data remains as each new point representing the behavior of a local region of that time series. It has a smoothing behaviour on the data which reduces the effects of noise.

There are two parameters in sliding window technique: Window length and the amount of sliding. Previous studies on prostheses have shown as window length increases, training performance increases [71, 72]. This also applies to the data used in this thesis study. However, an increase in window length also means using information from the future. On the other hand, this is meaningless for real-time applications. Therefore, a delay which corresponds to window length must be introduced to the system; so that statistical calculations can be done. The controller delay physically corresponds to time passing between the intent of the user and the actuation of the movement by the device. However, as controller delay increases, problems may emerge such as overshooting of the target for the prosthesis user which in turn increases the error. Therefore, there has to be an optimum value for window size which satisfies both theoretical and practical performance. According to the literature, 100-150 ms is generally accepted and used as window length [70, 73, 74]. On the other hand, there are also more loose window length criteria used in the literature. Xu et al. selected 300 ms long windows for a prosthetic arm design and Englehart et al. set the controller delay limit to 300 ms and selected an analysis window of 256 ms not to cross that limit [75, 76]. Another issue with the analysis windows is increment rate. Consecutive windows may or may not overlap, in terms of the step size of shifting. There is a common opinion that overlapping windows lead to higher performance [77]. However, there are studies on joint movement controller design using non-overlapping analysis windows [58, 78].

Considering the specifications in the literature and the effects on the proposed neural networks' performances, sliding windows having window lengths between 125-175 ms with increments of between 10-15 ms are recruited for this study. Although there are less conservative window lengths used in the literature, to be in line with real-time application purposes, it is aimed to stick with more conservative controller delay limitations in the literature as a design parameter. Controller delay problem can be determined more clearly if a prototype of the device would be manufactured. So that real time tests can provide actual results to tune this design parameter.

2.4 Feature Extraction

Taking the necessary information from raw data, especially from complex ones such as EMG signals, is a challenging task for artificial intelligence. Therefore, extraction of the required features that reveals the information remaining in depths of raw EMG before feeding it to the neural network becomes a key process for enhanced performance. Hence, feature extraction allows the network to get more information from the same sensor inputs.

It is shown that a well-worked feature extraction improves the performance significantly [79, 80]. After observing that raw EMG signals were not sufficient as input set, feature extraction was applied.

In general, there are time domain features and frequency domain features. Main focus of areas while using frequency domain features include muscle motor unit employment and muscle fatigue which is not main focus of this study [81]. While frequency domain features require the conversion of time domain data to frequency domain using methods such as FFT, time domain features are extracted from time series data [82]. Therefore, time domain features are mostly simpler in terms of computation. Due to real-time application aim, use of time domain features is addressed in this study. Hudgins et al. came up with 4 time domain features for myoelectric signals in 1993 [83]. They are slope sign changes (SSC), mean absolute value (MAV), zero crossings (ZC) and mean absolute value slope (MAVS). They have been used a lot for EMG signals in the literature. At first, these 4 features were used as a basis to develop the network. Subsequently, other time domain features have been researched to improve the performance in terms of feature set. Phinyomark et al. investigated the effects of some features on a classification task for the control of upper limb prostheses [84]. The success rates of the features and rankings relative to each other change with varying window lengths. Thus, there is not a certain best feature set, the success rate can change due to changes in the conditions. However, it can be seen in the results of the study in the Feature Selection section that there are some similarities between the results of both Phinyomark et al. and this thesis. Because of these inferences, it is

decided to make a separate test on the data to be used, considering the results of the previous studies on feature selection for EMG signals.

2.5 Feature Selection

The advantages of feature extraction are mentioned in the previous section. However, an increase in the number of features does not always mean that the results will increase. It is not an ideal way of training a network to feed the network with all of the features. Moreover, a reduction in the number of input channels leads to improvement of efficiency by reducing computational time. Therefore, there should be an optimal combination of input features for a system.

A feature selection analysis is performed with the aim of finding the ideal features. Performance can be improved by avoiding complexity by eliminating the redundant input components [85]. In addition, computational cost of both training process and real-time use is aimed to be reduced by finding the minimum number of features required. Decreasing the volume of a data in the according space so that there is only a volume left which represents the essence of the data is called dimensionality reduction. Feature selection is a part of dimensionality reduction [81, 86].

There are different methods used for feature selection in the literature. Tkach et al. investigated the stability of feature sets against introduced disturbances starting with testing the individual features, then continued with the combinations of features with different sizes and features [87]. With a preliminary study and literature research, the number of potential features is reduced to 8: Mean absolute value (MAV), waveform length (WL), slope sign changes (SSC), Willison amplitude (WAMP), modified mean absolute value (MMAV1), integrated EMG (IEMG), root mean square (RMS) and variance of EMG (VAR). The equations for all is in Appendix.

Afterwards, an analysis is performed to determine the optimal number of features. The results are shown in Figure 2.3. It should be noted that this approach

includes only one muscle combination, i.e. TA and MG. Although the results would change for different muscle combinations, these variances are assumed not to be significant. Feature set of 3-features is selected, since there is not a significant improvement after increasing the number of features more than 3. Remember that an increase in the number of features would yield a more complex structure.

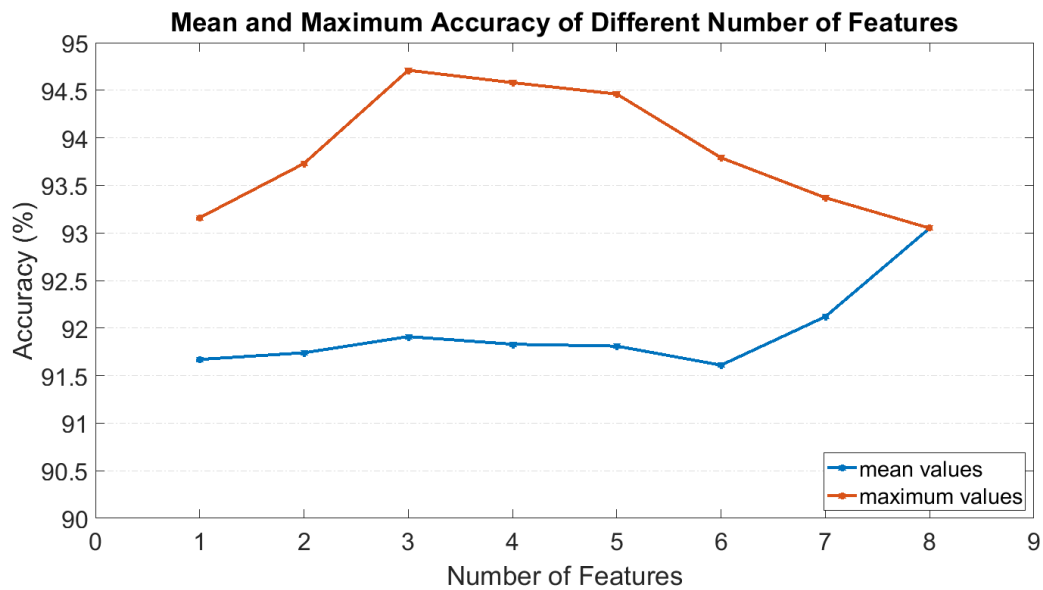


Figure 2.3 Comparative results of the feature sets with different sizes.

An intra-class correlation analysis is performed to understand the features of EMG data used in this study. The aim is to detect the linearities between input features to eliminate highly dependent features to avoid multicollinearity. Parallel to this, increasing the network performance by avoiding multicollinearity. The results of this approach are in Figure 2.4 and 2.5.

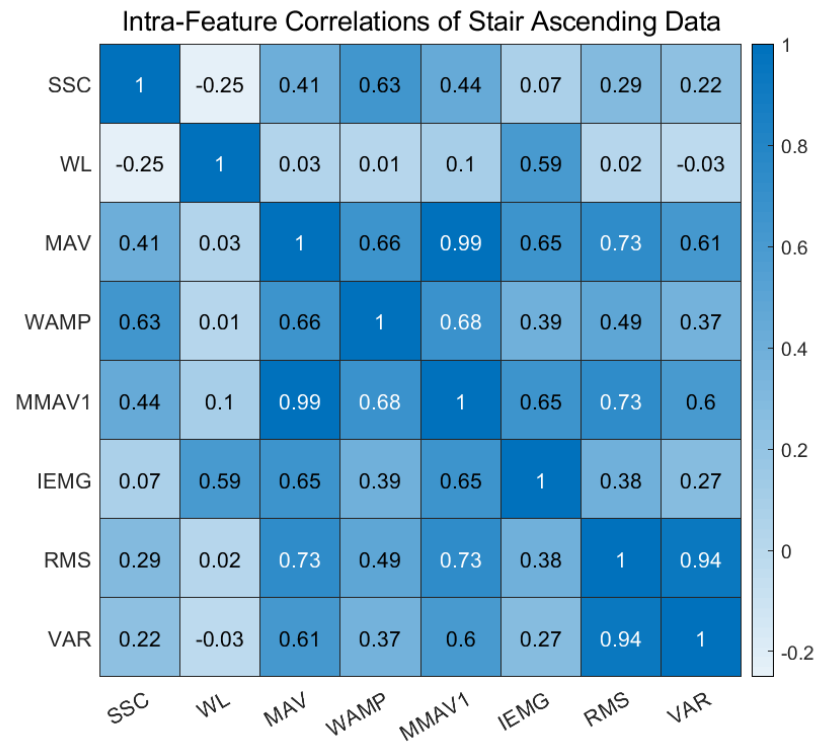


Figure 2.4 Intra-feature correlation analysis results for stair ascending. The darker the color the higher the correlation.

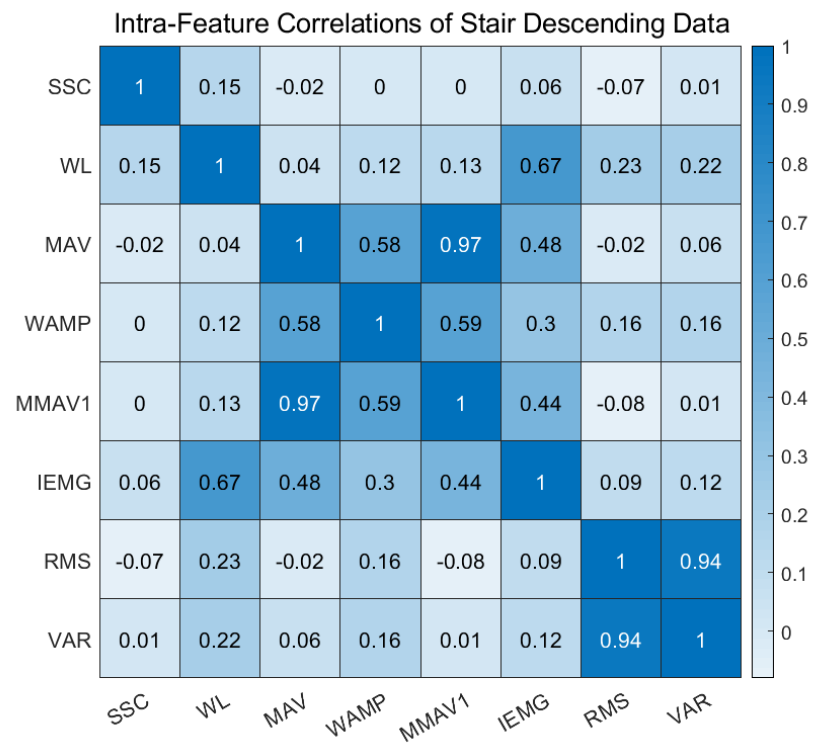


Figure 2.5 Intra-feature correlation analysis results for stair descending. The darker the color the higher the correlation.

It is noteworthy that there is a quite much difference in the correlation results between two tasks. Features in stair ascending are much more dependent on each other. The reason for this distinction may be the relations between muscle activations of two tasks.

To conclude, intra-features correlation study shows that some features are highly linearly dependent. The following observation would not be surprising by a look at the statistical formulas of the features. It can be convincingly said from the intra-feature correlation results that MAV, MMAV1 and slightly IEMG are kind of different versions of each other. Therefore they would contribute to the feature set from a close perspective. Similarly, RMS and VAR are highly related with ρ value of 0.94. Although SSC could present information related to signal frequency characteristics which is different from other features that is also indicated by intra-features correlation study, it was not in the feature combinations with the best results [87]. MAV, IEMG, RMS and VAR are the most frequent features that appear in the feature sets with the best results. Despite being observed that WAMP is not one of the most seen features in the best-performing combinations, it is a component of the best performed set. WAMP is a measure which counts the exceeding a certain threshold of the change in EMG amplitude. It can represent the motor unit action potential firing rates and the level of muscle contraction. In the work of Phinyomark et al., WAMP is the feature with the best performances. A threshold of 10 mV is set for WAMP. As the voltage threshold decreased within the range of 5-50 mV, WAMP performance had increased. It is shown to perform well with signals having white noise which is an important issue in sEMG signals [88]. WAMP is calculated as follows:

$$WAMP = \sum_{n=1}^{N-1} f(|x_n - x_{n+1}|) \quad (2.1)$$

where

$$f(x) = \begin{cases} 1 & x \geq threshold \\ 0 & otherwise \end{cases} \quad (2.2)$$

In Eq. 2.1, x_n and N denote n^{th} raw EMG and the length of the signal, respectively.

RMS can represent the EMG power [89]. It is able to produce the maximum likelihood estimation of the amplitude of the signal [81]. It is shown in Ajiboye et al. that RMS can provide a significant representation from EMG signal [90]. The formula for RMS is in Eq. 2.3.

$$RMS = \sqrt{\frac{1}{N} \sum_{n=1}^N x_n^2} \quad (2.3)$$

After rectification, MAV is a measure that shows the area under the EMG amplitude. It can represent EMG signals so well that the study of Zarshenas et al. on ankle torque prediction uses only MAV to represent EMG signals, but also with kinetics and kinematics inputs [74]. The equation for MAV is below.

$$MAV = \frac{1}{N} \sum_{n=1}^N |x_n| \quad (2.4)$$

In consequence, MAV, RMS and WAMP are selected as elements of a set of 3 features to be extracted from EMG input data. If it is desired to further decrease the number of features, MAV and RMS would provide successful results.

2.6 Muscle Combinations

The selection of the muscle combination with the greatest performance is not as simple as the feature selection process. Each muscle contributes in a unique manner in the biomechanics of human movement, whereas the features are statistical calculations to represent EMG signals which is a more generalizable concept.

There are 4 outputs: Step up moment, step up angular position, step down moment and step down angular position. Muscle activation distribution depends on both gait task and the subject of prediction, i.e. position and moment. Therefore, it would not be surprising that if the results yield different optimal sEMG sensor sets for each type of output. Despite that there is a detailed study whose results are presented in the Results section, a preliminary study on the muscle activations is performed to have a wider view on the problem. It is an intra-muscle analysis which is similar with the aforementioned intra-feature analysis. The aim is to bring a perspective to the final results by digging deep the nature of the muscle mechanics. The intra-muscle correlations is shown in Figure 2.6 and 2.7.

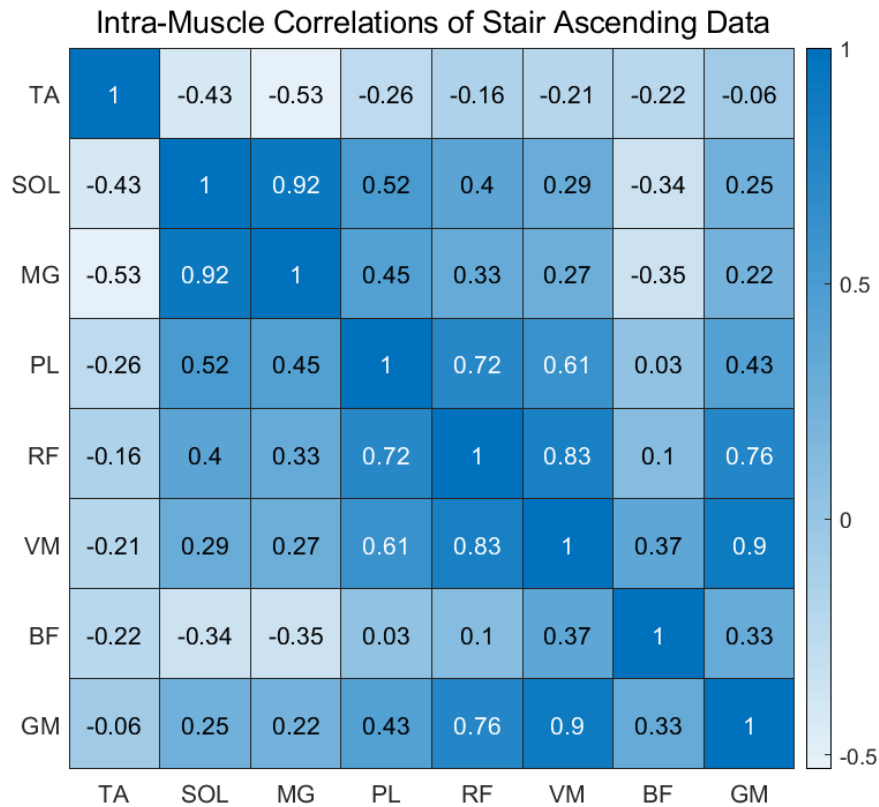


Figure 2.6 Intra-muscle correlation analysis results for stair ascending.

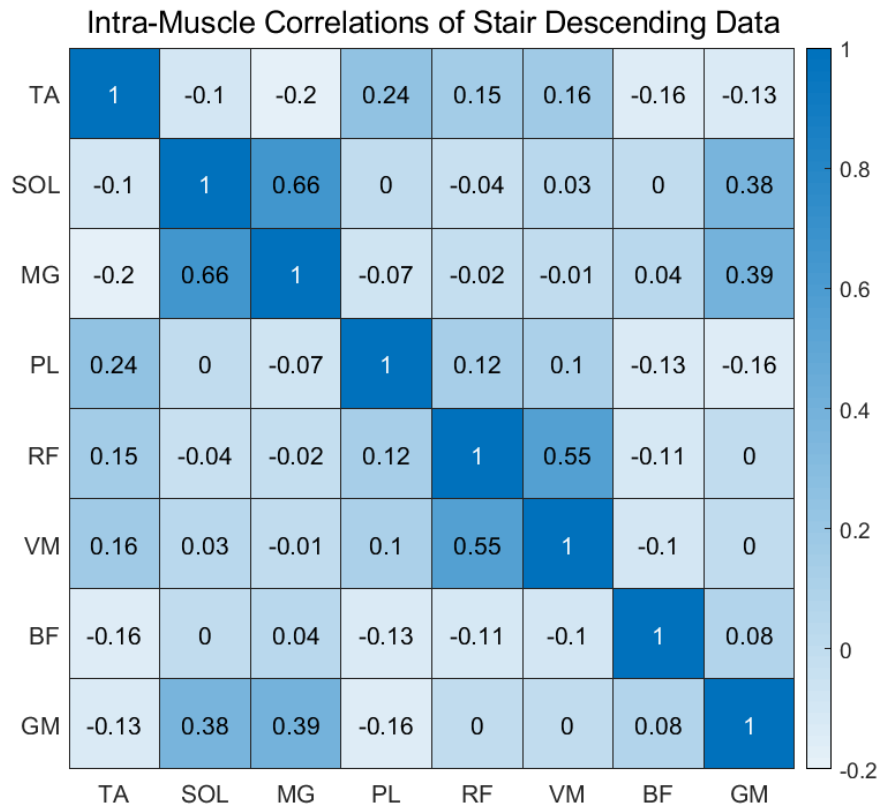


Figure 2.7 Intra-muscle correlation analysis results for stair descending.

Firstly, the evaluation of Figure 2.4 and 2.5 with Figure 2.6 and 2.7 reveals the strength of the relationship between muscles in stair ascending and descending tasks. It is denser in stair ascending. About specific intra-muscle dependencies, SOL and MG of calf muscles have the highest correlation value in both tasks. RF and VM also have high correlation values in both tasks. Furthermore, RF-VM which are the parts of quadriceps muscles, VM-GM and RF-GM relations can be mentioned as strong for stair ascending.

2.7 Neural Networks

The problem definition is regression of time series data. Accordingly, neural network architectures for this type of problem have been researched. Time delay neural network (TDNN) and long short-term memory (LSTM) are decided to be used in this study.

2.7.1 TDNN

TDNN is a previously used neural network type for gait data [63]. TDNN can be mentioned as an extended multilayer perceptron. To be more specific, it is a feed-forward network except with an additional element which is called time-delay. Time-delay concept allows artificial neurons of hidden layer or output layer to get information from the previous M inputs. In this way, it can link the information of the past and current time to predict future output values [91]. The main idea behind TDNN can be formulated as follows:

$$y(k) = f(u(k), u(k-1), \dots, u(k-M)) \quad (2.5)$$

where $y(k)$ is the output at time k , $u(k)$ is the input, and M is the maximum adopted time-delay.

TDNN has a structure which is good at handling temporal patterns. Human joint behavior estimation is a complex task. Bayesian regularization backpropagation algorithm is selected as a training function. It is better at modeling complex relations than its alternatives such as the Levenberg-Marquardt algorithm [92]. Jacobian matrix is used in this method and sum of squared errors for the optimization of performance. Additionally, its objective function includes sum of squared weights and penalizes too complex model structures. Therefore, it is good at generalization [92, 93]. The block diagram of TDNN is in Figure 2.8.

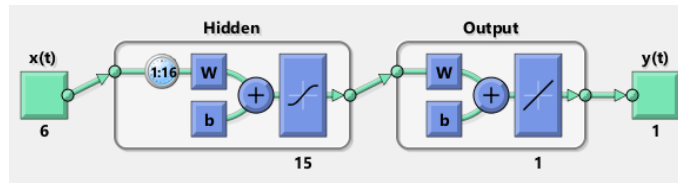


Figure 2.8 An illustration of TDNN structure. Generated via Matlab.

2.7.2 LSTM

LSTM is a deep learning method which is a form of recurrent neural network (RNN) architecture. It is one of the popular methods used in time series forecasting in real-time [94]-[95]. It learns very fast compared to backpropagation through time. It also has good generalization ability. In addition, it can recognize long-term dependencies in time series data.

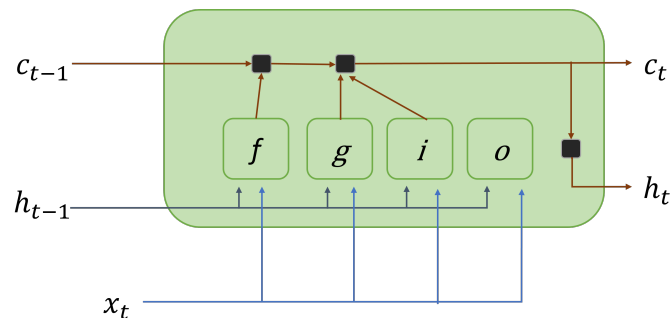


Figure 2.9 An illustration of an LSTM block showing the flow of data through gates.

To explain the LSTM working principle, there are cell state and corresponding gates. Cell state allows the information of previous time steps to be carried on to later time steps. As sequence data flows, gates remove or add information to the cell state. There are forget gate, input and output gates. Forget gate decides which information will be removed or kept. Input gate updates the cell state. The output gate determines the hidden state. There is an illustration of this principle in Figure 2.9 and the mathematical representation of this process is in Eq. 2.6-2.11.

$$c_t = f_t \odot c_{t-1} + i_t \odot g_t \quad (2.6)$$

$$h_t = o_t \odot \sigma_c(c_t) \quad (2.7)$$

where c_t and h_t denote cell state and hidden state at time t , respectively.

$$i_t = \sigma_g(\omega_i X_t + R_i h_{t-1} + b_i) \quad (2.8)$$

$$f_t = \sigma_g(\omega_f X_t + R_f h_{t-1} + b_f) \quad (2.9)$$

$$g_t = \sigma_c(\omega_c X_t + R_g h_{t-1} + b_g) \quad (2.10)$$

$$o_t = \sigma_g(\omega_o X_t + R_o h_{t-1} + b_o) \quad (2.11)$$

where i_t , f_t , g_t and o_t denote input gate, forget gate, cell candidate and output gate at time t , respectively. And W , b and R are input weights, bias and recurrent weights of corresponding gate, respectively.

2.7.3 Hyperparameter Optimization

Hyperparameter tuning of the model is an essential process for neural network development. It enhances the performance of the model. Computational cost should also be taken into account while improving the performance. Therefore, the significance of the improvement in the performance is also considered if it is more efficient in terms of time consumption. A too simple network would cause an underfitting of the data, whereas a too complex network would result in overfitting to training data. Therefore, test results would be decreased.

There are 5 hyperparameters for TDNN: Time-delay, number of iterations, number of hidden units, number of hidden layers and the type of training function. While developing TDNN, design limitations about real-time application affected time-delay, and sliding window length. TDNN performance is highly dependent on both of them.

Hyperparameters of LSTM are initial learning rate, dropout rate, number of hidden layers, number of hidden units, number of epochs, mini batch size and L2 regularization constant.

Stochastic optimization methods are generally advantageous among others using the nature of randomness with its ability to avoid local minima and its performance in complex problems [96]. One of the stochastic optimization methods is Adam optimizer. It is selected as the solver of LSTM. Main advantages of Adam are computational efficiency and its success in non-stationary data [97]. At first, overfitting was a problem that limits the network performance. To avoid overfitting to training data, it is shuffled in every epoch. Another prevention for overfitting is dropout. Additionally, use of L2 regularization is investigated in Bayesian optimization.

Hyperparameters can be optimized by grid search or random search techniques. Grid search is a rough method which can be hard to handle a wide range of parameters. It is shown that random search outperforms grid search regarding both time consumption and performance. Its ability to avoid local minima plays a key role in this comparison [98].

As a result of hyperparameter optimization, for TDNN, 1 hidden layer with 15 hidden neurons is selected. Design criteria of sliding window length and the amount of time-delay limited the performance of TDNN. To be more clear, if these parameters were increased above the design limits, the performance would improve. On the other hand, even if the limitations on the analysis window were not required to be exceeded, LSTM provided sufficient results even with windows of 75 ms length. Despite the fact that a standardized set of hyperparameters for all output types was leading to satisfactory results, different hyperparameters are used for different targets to improve

the results. Initial learning rate is between 0.0025-0.0040, dropout rate is 0.6, number of hidden units is 51, number of epochs change between 100-177, L2 regularization constant is between 0.0005-0.00001 and mini batch size is between 12-36. It is better to start with simpler models and make it more complex until reaching the targeted performance. A fully connected layer consisting 50 hidden units is found to be sufficient to keep the simplicity in the architecture. The structure of the proposed LSTM network is illustrated in Figure 2.10.

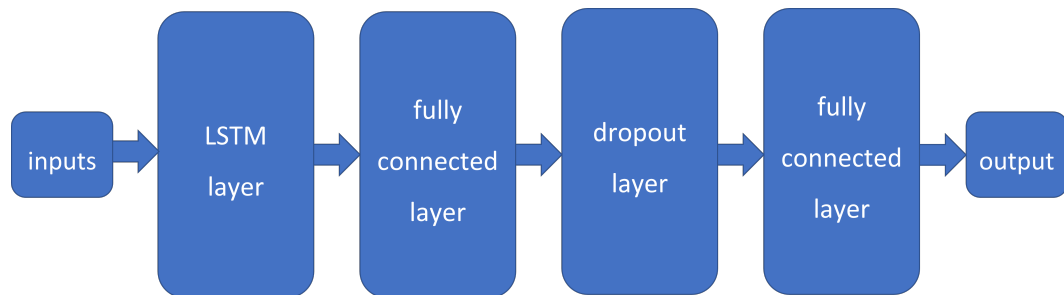


Figure 2.10 The structure of the proposed LSTM network.

To improve hyperparameter selection, another optimization technique called genetic algorithms (GAs) can be examined. GAs can optimize stronger than Bayesian optimization in means of finding the global minima [99]. Another study on the types of GAs may lead to finding better resulting hyperparameters.

2.7.4 The Comparison of TDNN and LSTM

At first, TDNN and LSTM are trained with input combinations consisting of different number of muscles to make a comparison. For instance, there are 28 different input sets consisting of 2 muscles in total, and 56 input sets consisting of 3 muscles. The performance of both neural network architectures with varying input sets is analysed. In this way, the behavior of each architecture can be observed by changing the input information and the overall advantageous architecture can be determined.

The finding of this comparison is shown in the Results section. Subsequently, LSTM is recruited which has higher accuracy results and much lower computational cost.

2.8 Five-Fold Cross Validation

Validation technique can have a substantial effect on the results [100, 101]. To assess the generalizability of the proposed models, cross validation is applied to data sets. The aim is to avoid the biases in the distribution of data set into training and test data subsets. A more generalized solution to the stated problem of the study can be achieved by applying cross validation.

There are various cross validation methods. One of them is k-fold cross validation which is a commonly used technique [102]. In k-fold cross validation, samples are divided into k groups. Then the network is trained with k-1 groups and tested by one group. This is repeated k times to evaluate the performance of the model with each sample group separately. Finally, performance measures of each repetition are averaged to obtain the most generalized solutions. k-fold cross validation uses all samples in training and performance evaluation and there are not any overlapping samples in the groups which helps avoiding bias. $k = 5$ is selected considering both generalizability and computational cost.

2.9 Performance Evaluation

The accuracy in imitating a healthy gait cycle determines the success of such an algorithm for a device. Two test statistics are used as a performance measure: Root mean square error (RMSE) and Pearson's correlation coefficient (ρ). Root mean square error is the sum of squared differences between the predicted and the actual outputs divided by the sample size. It is in units of degrees for position, and Nm/kg for moment output. Pearson's correlation coefficient is a statistical measure of the linear association between the predictions and real values.

$$RMSE = \sqrt{\sum_{t=1}^n \frac{(\hat{y}_t - y_t)^2}{n}} \quad (2.12)$$

where n is sample size and y_t and \hat{y}_t denote the predicted and the actual output values at time t , respectively.

$$\rho(\hat{Y}, Y) = \frac{cov(\hat{Y}, Y)}{\sigma_{\hat{Y}}\sigma_Y} \quad (2.13)$$

where covariance cov is defined as

$$cov(\hat{Y}, Y) = \frac{1}{N-1} \sum \left(\frac{\hat{Y}_t - \mu_{\hat{Y}}}{\sigma_{\hat{Y}}} \right) \left(\frac{Y_t - \mu_Y}{\sigma_Y} \right) \quad (2.14)$$

Y and \hat{Y} denote a sample and the prediction of it, respectively. μ and σ are the mean and standard deviations, respectively. N is the length of the sample.

For a control algorithm to be counted as successful, basically it should be functional, but not make difficulties for the user. Real time tests on devices which targeted users wear could also set better criteria on success. Yet there are some specifications on performance evaluation in the literature for preliminary studies such as this thesis aiming to lead to final devices. According to the literature, correlation coefficient of 0.90 between the predicted and the actual values of human joint behavior [21, 53, 103, 19].

3. RESULTS

The final results for various scenarios are presented in this section. Distribution of the data as training and test data sets is totally randomized to avoid possible biases of handmade distribution.

3.1 The Comparison of TDNN and LSTM

The comparative results of both architectures with the 2-, 3- and 4-muscle combinations for position and moment estimations of stair ascending task are shown in Figure 3.1 and Figure 3.2, respectively.

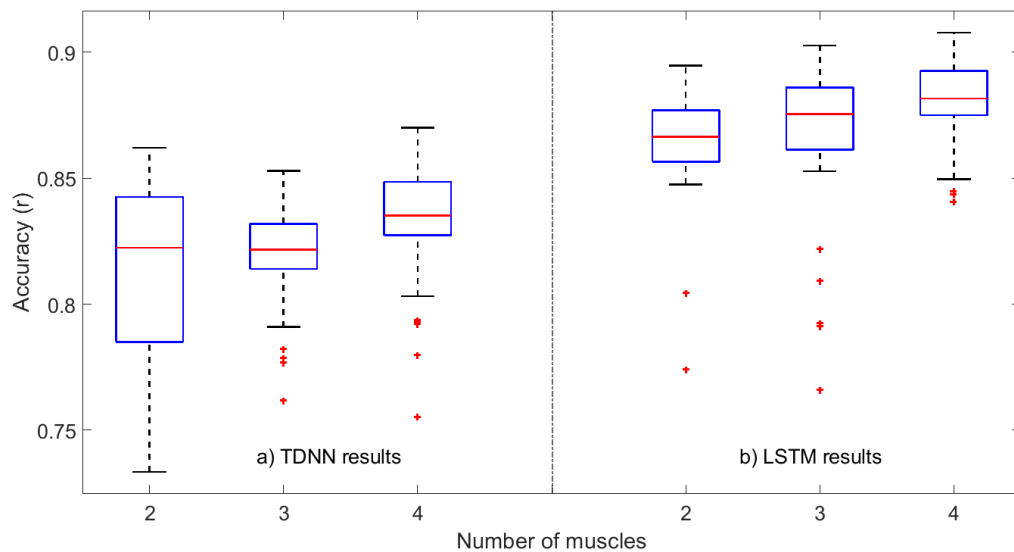


Figure 3.1 Box plot of stair ascending position prediction results of input sets with different number of muscles for comparison of a) TDNN, b) LSTM.

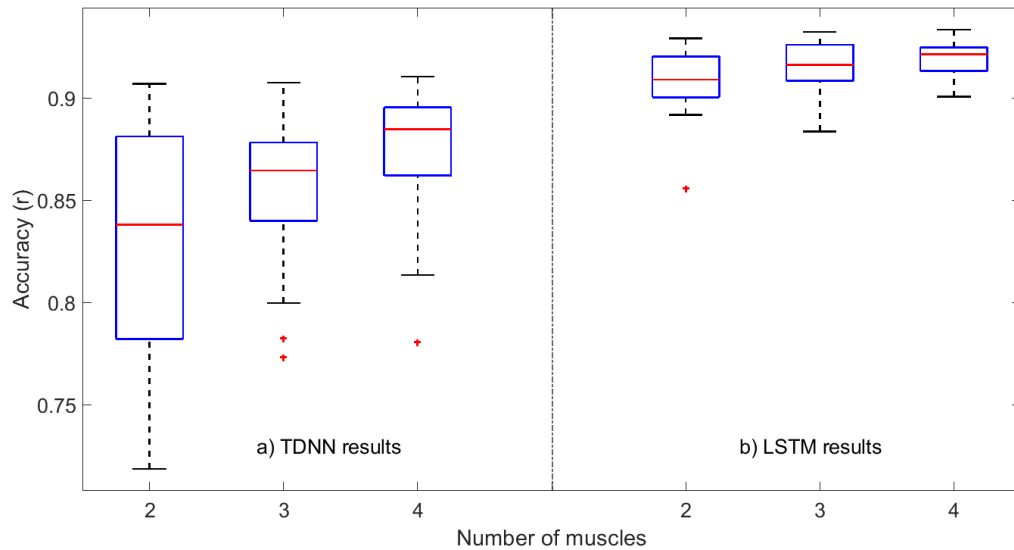


Figure 3.2 Box plot of stair ascending moment prediction results of input sets with different number of muscles for comparison of a) TDNN, b) LSTM.

The results of input sets consisting of only 1 muscle is not given in Figure 3.1 and 3.2, because TDNN could not even get close to satisfactory results. Paired t-test is conducted to assess the significance of the difference of TDNN and LSTM results. As a result, LSTM accuracies are significantly higher than the ones of TDNN ($p < 0.001$). Considering with its superiority in performance and time consumption, the rest of the study recruits LSTM. Therefore, the rest of the results given in this section were obtained with LSTM models.

3.2 Stair Ascending

3.2.1 Position Estimation

The results for position estimation are presented in this section in a similar way with the presentation of moment estimation results. The results are given in Figure 3.3. As the number of muscles in the input set increases, performance keeps increasing for stair ascending position estimation.

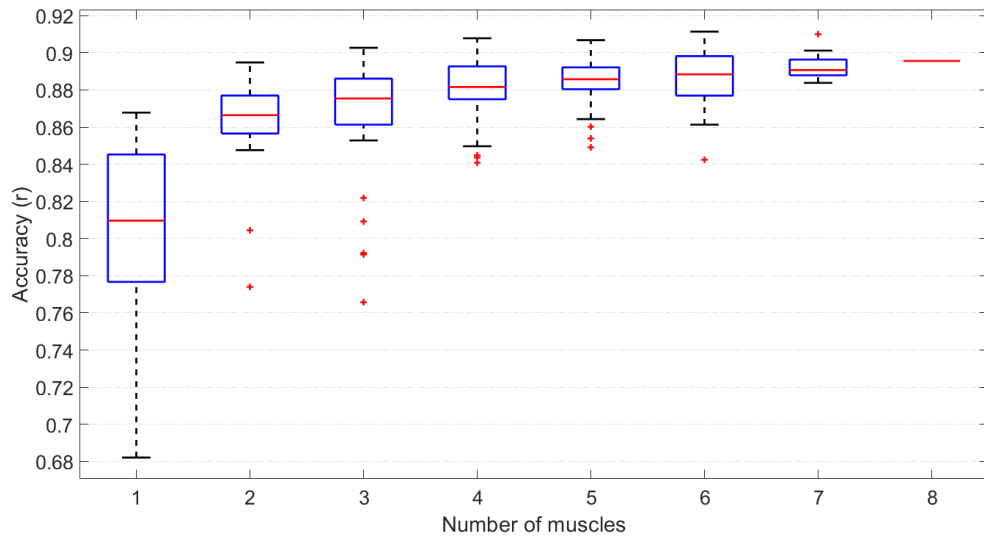


Figure 3.3 Box plot of position prediction results of input sets with different number of muscles for stair ascending.

3.2.2 Moment Estimation

The box plots of moment prediction for stair ascending task representing the shape of the performance distribution of each muscle set size are in Figure 3.4.

Unlike the position estimation, the accuracy does not significantly improve with the increase in the number of muscles in the input set more than 3-4 muscles, in terms of mean accuracy values. On the other hand, input sets of 6 muscles include the combinations with the maximum performance for stair ascending.

Paired t-tests within each number-of-muscles group were conducted to assess the relationship between position and moment estimation results. According to paired t-tests, moment prediction accuracy results are significantly higher than position predictions ($p < 0.001$) with the exception of 7-muscle combinations for stair ascending ($p > 0.01$).

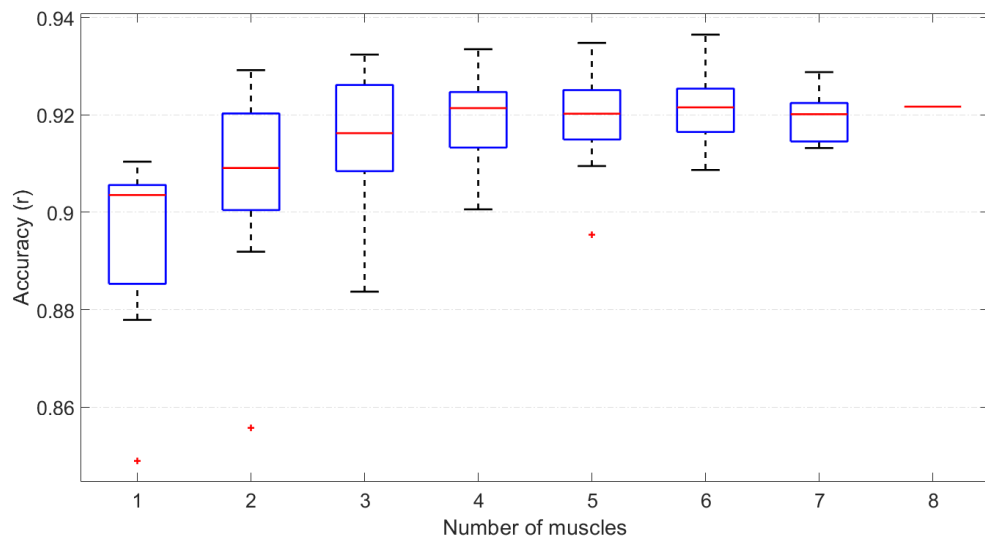


Figure 3.4 Box plot of moment prediction results of input sets with different number of muscles for stair ascending.

3.3 Stair Descending

3.3.1 Position Estimation

The position estimation results for stair descending is shown in Figure 3.5.

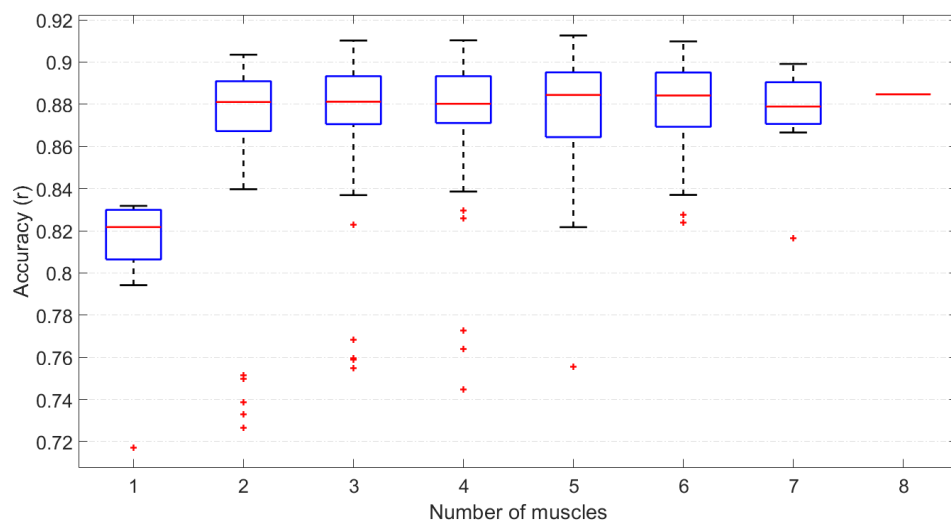


Figure 3.5 Box plot of position prediction results of input sets with different number of muscles for stair descending.

Unlike the position prediction results of stair ascending task, performance does not improve continuously while increasing the number of muscles in the input set.

3.3.2 Moment Estimation

Moment estimation results for stair descending is shown in Figure 3.6.

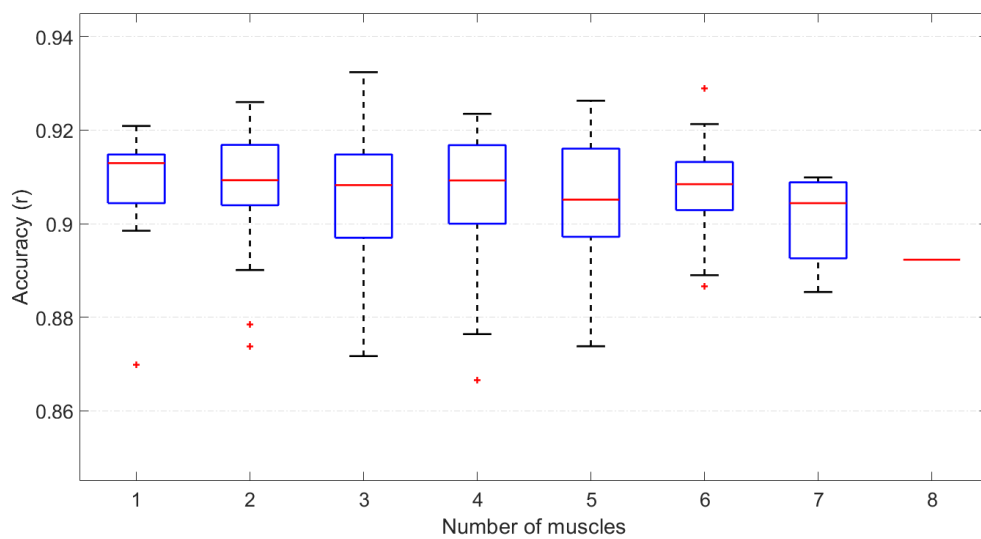


Figure 3.6 Box plot of moment prediction results of input sets with different number of muscles for stair descending.

Similar to stair ascending, moment prediction results does not significantly improve after some point. After 2- and 3-muscle combinations, increasing the number of muscles in the input set does not seem effective.

According to paired t-tests, moment estimation results are significantly higher than the position estimations ($p < 0.001$) with the exception of the 1-muscle combinations for stair descending ($p > 0.01$). Further statistical tests indicate that the level of the significance of the difference between stair ascent and descent varies. 1- and 2-muscle combinations do not show a significant difference for both outputs ($p > 0.5$). On the other hand, for the remaining sets stair ascending accuracy results are significantly higher than stair descending for moment prediction ($p < 0.005$). Position prediction

accuracies of muscle sets which are consisting more than 3 muscles for stair ascending are also significantly higher than stair descending, but the significance level is lower ($p < 0.1$).

3.4 Best-Performing Variations

In this section, the muscle combinations with the best performance are presented.

In Table 3.1, there are the best position predictions among the results which considered as sufficient. It can be seen that there is not any input set without TA among 30 combinations with the highest accuracy for ankle position estimation. SOL and MG are also frequent in Table 3.1.

Table 3.1

The 15 best position prediction results. Stair ascending on the left, stair descending on the right.

Stair Ascending Position			Stair Descending Position		
Muscle set	ρ	RMSE	Muscle set	ρ	RMSE
TA, SOL, MG, PL, BF, GM	0.9114	2.608±1.3211	TA, SOL, MG, RF, VM	0.9126	2.6953±1.2551
TA, SOL, MG, PL, RF, BF, GM	0.9101	2.618±1.2905	TA, MG, PL, RF, BF	0.9124	2.4872±1.2276
TA, SOL, PL, BF	0.9078	2.5956±1.3406	TA, MG, RF, VM, BF	0.9117	2.8456±1.1641
TA, PL, RF, BF, GM	0.9068	2.5522±1.2182	TA, MG, PL, RF	0.9103	2.8267±1.2728
TA, SOL, PL, RF, BF	0.9051	2.7053±1.3573	TA, MG, BF	0.9102	3.0119±1.1593
TA, SOL, MG, GM	0.905	2.5892±1.3873	TA, SOL, PL, RF, VM, GM	0.9098	2.9346±1.1984
TA, MG, PL, BF	0.9049	2.5763±1.3507	TA, MG, VM, BF, GM	0.9091	2.9440±1.2013
TA, SOL, MG, PL, RF, GM	0.9038	2.5756±1.3079	TA, MG, VM	0.9083	3.0205±1.2073
TA, MG, BF, GM	0.9037	2.6553±1.4698	TA, SOL, PL	0.9075	3.0600±1.3524
TA, SOL, MG, PL, RF	0.9028	2.5771±1.3475	TA, SOL, MG, VM, GM	0.9075	3.0691±1.1228
TA, SOL, MG	0.9027	2.6108±1.3724	TA, SOL, MG, RF, VM, BF	0.9071	2.9296±0.9954
TA, SOL, MG, RF, BF, GM	0.9015	2.6062±1.3843	TA, SOL, PL, RF, VM, BF	0.9065	2.9543±1.0907
TA, SOL, PL, GM	0.9014	2.6578±1.3573	TA, PL, RF	0.9059	2.9924±1.0858
TA, SOL, MG, PL, VM, BF, GM	0.9012	2.6269±1.4471	TA, MG, RF	0.9057	3.0650±1.1314
TA, SOL, PL, RF, BF, GM	0.901	2.5517±1.3053	TA, MG, PL, VM	0.9055	2.9171±1.2732

Table 3.2

The 15 best moment prediction results. Stair ascending on the left, stair descending on the right.

Stair Ascending Moment			Stair Descending Moment		
Muscle set	ρ	RMSE	Muscle set	ρ	RMSE
SOL, MG, RF, VM, BF, GM	0.9365	0.0872±0.0533	MG, RF, BF	0.9324	0.1169±0.0701
TA, MG, PL, RF, GM	0.9348	0.0883±0.0508	TA, MG, VM	0.9296	0.1176±0.0711
TA, MG, RF, VM	0.9335	0.0876±0.0468	TA, MG, PL, RF, VM, BF	0.9289	0.1214±0.0698
TA, MG, PL, RF, VM, GM	0.9332	0.0930±0.0482	TA, SOL, MG, VM, BF	0.9263	0.1199±0.0691
TA, SOL, MG, RF	0.9326	0.0865±0.0481	MG, VM	0.9260	0.1188±0.0700
TA, SOL, VM	0.9324	0.0911±0.0499	MG, BF, GM	0.9250	0.1189±0.0692
SOL, MG, GM	0.9324	0.0922±0.0564	TA, MG	0.9239	0.1196±0.0702
SOL, MG, RF	0.9323	0.0868±0.0514	MG, BF	0.9237	0.1165±0.0698
TA, SOL, MG, PL, VM	0.9320	0.0904±0.0542	SOL, VM	0.9236	0.1202±0.0693
SOL, MG, PL, RF, VM, GM	0.9316	0.0860±0.0511	TA, MG, RF	0.9235	0.1173±0.0661
MG, PL, VM	0.9314	0.0911±0.0526	TA, SOL, MG, RF	0.9235	0.1170±0.0720
SOL, MG, VM	0.9312	0.0895±0.0547	TA, MG, PL, RF	0.9232	0.1165±0.0655
SOL, MG, PL, VM, GM	0.9308	0.0872±0.0522	SOL, MG, PL, RF, BF	0.9232	0.1232±0.0755
MG, PL, RF, VM	0.9303	0.0894±0.0508	TA, SOL, MG	0.9228	0.1184±0.0708
TA, MG, VM, BF, GM	0.9301	0.0888±0.0503	SOL, MG, RF, VM, BF	0.9228	0.1204±0.0740

The results for moment estimation with the greatest accuracy is shown in Table 3.2. Moment estimation accuracy around 93% is reached with various muscle sets for both focused movement tasks. There is not any muscle combinations without either SOL or MG in Table 3.2. There are more combinations including less muscles for the moment estimation of stair descent compared to stair ascent.

In Figure 3.7 and 3.8, the comparison of the predictions of the models and the actual values is shown. Lines represent mean values and the shaded areas show mean values ± 1 standard deviation. Although the mean values are close, the variations of the actual values can be observed.

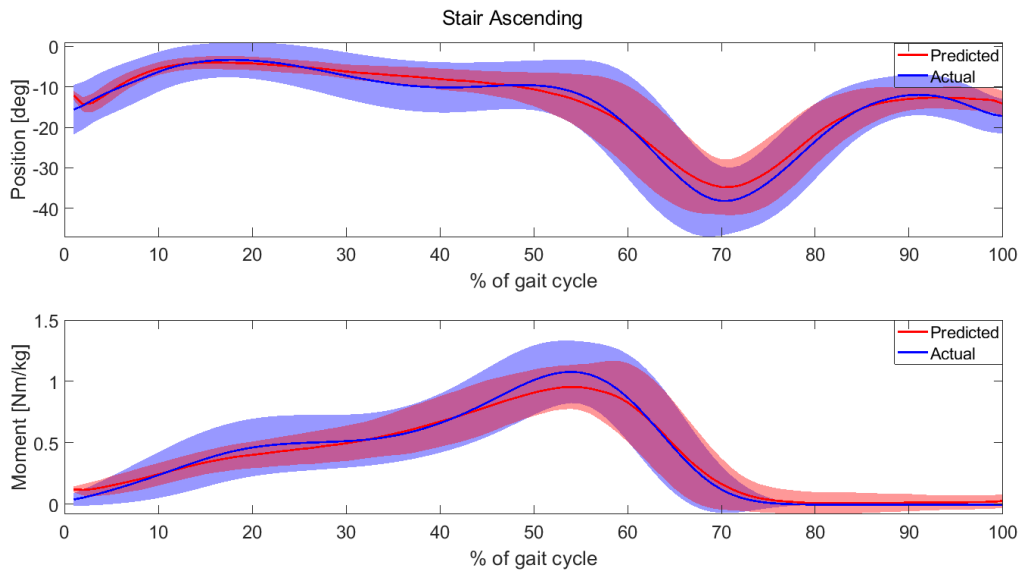


Figure 3.7 Stair ascending predictions vs actual values of the best-performing muscle combination.

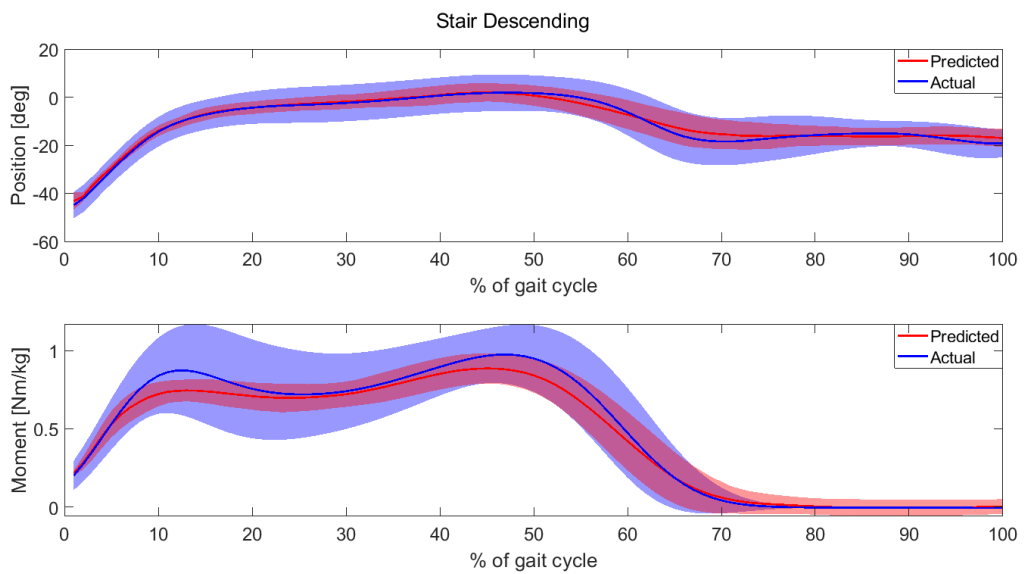


Figure 3.8 Stair descending predictions vs actual values of the best-performing muscle combination.

4. DISCUSSION AND CONCLUSION

Estimation of ankle position and moment for stair ascending and descending tasks makes four different objectives in this study. Despite the fact that all are a part of stair ambulation, the differences in ascending and descending reflected into results. Moment and position estimations also differed. As a result of the study, some models achieved successful accuracy.

Feature selection for myoelectric signals is an interest of research. Despite being similar in terms of the nature of muscles, the ideal feature sets representing myoelectric signals vary in the literature. Therefore, an initial study to obtain an optimal set of features was performed and it verified the statement mentioned in the last sentence. Besides the selected features, the performances of other feature combinations are given in the Appendix. Hopefully, it would be beneficial for the upcoming researches on similar topics.

Even if there is not a gold standard for such human joint predictor design for smart prostheses, a correlation coefficient (ρ) between the predicted and the actual values of 0.9 and mean relative error (MRE) of 0.15 can be set as an acceptance limit for human joint behavior predictors of smart prostheses which is considered reliable and valid [21, 53, 103, 19]. Therefore, correlation coefficient of 0.9 was set as the performance threshold for this study. Although there are studies that show results lower than these limits yet experimented with sufficient performances [27, 104]. It is still a convenient way to set performance limits in engineering studies to enhance the work by doing it in a more challenging and less risky way. Consequently, correlation coefficient of 0.90 between the predicted and the actual output values, instead of the one used as 0.95 in Keles and Yucesoy [63].

At first, two neural network architectures were compared. TDNN was used in Keles and Yucesoy. However, TDNN performance was not satisfactory for the data and

tasks focused in this study. Considering computational time and efficiency, only 2-,3- and 4-muscle combinations for stair ascending were examined for the comparison of the two architectures. According to the results of Keles and Yucesoy, TDNN were more successful with the input variations of more muscles. Since more muscles would mean less difference, the input sets with less muscles were more essential in this selection [63]. Consequently, LSTM architecture resulted in greater overall accuracy than TDNN. Although some input combinations for TDNN crossed the 0.90 correlation threshold which was defined for this study, the performance distribution characteristics were significantly below LSTM. The main reason for the lower performance of TDNN is window length and time-delay restrictions. Also, the interpolated number of data points affected. It could achieve higher accuracy results with increased number of data points which may compete with LSTM performance for the specified problem statement of this thesis study. The main behaviour in the lower performance of TDNN was overfitting to training data sets. Prasertsakul et al. faced the overfitting problem in a nonlinear autoregressive exogenous model (NARX) which is similar to TDNN with a feedback loop that enables the use of the information from the past values of the output [105]. The results show that more sensory information does not always mean more accuracy as expected in the Methods section. The reason for this can also be overfitting and multicollinearity problems. Additionally, TDNN required analysis window length of at least 175 ms to produce some above-threshold results while LSTM models were trained with 125 ms windows and even 75 ms window length gave successful results which was not selected not to decrease overall accuracy.

Another difference of this study from Keles and Yucesoy is the number of muscles which the data set includes. SOL, PL and VM are the additional muscles of the data set used in this study [63]. EMG input set requirements for the best results differed for each objective. It means the relationships between the muscle activations and ankle kinetics and kinematics differs. Therefore, output-specific solutions should be applied for the optimal results for each one. This means the target with the requirement of the highest number of sEMG sensors would determine the mechanical and electronic system design requirements.

There are 239, 190, 16 and 27 above-threshold muscle sets for respectively stair ascending moment, stair descending moment, stair ascending position and stair descending position outputs. It is obvious that position prediction is harder than moment prediction for the proposed networks.

For the use of minimum number of sensors aim which makes the prosthesis more economic, TA and MG could be satisfactory for the all targets except position estimation during stair ascending. For position of stair ascending, TA+MG combination resulted with an accuracy of 0.8948 which is near to the threshold. According to the results, the addition of PL and BF makes the combination sufficient for all tasks.

Lower leg muscles are the most frequently seen input components of the above-threshold combinations. The differences in the nature of transtibial amputations can affect the sufficiency of the EMG signal to be collected from the residual muscles. Due to this variability, the use of upper leg muscles' EMG signals could be more preferred. On the other hand, the use of only lower leg muscles can be advantageous for a prosthetic device that is worn only to the residual tissue of the body. It would prevent the additional sensors on the sound parts of the user's body. The study of Au et al., 2008 shows that it is possible to use only lower leg muscles in ankle-foot prosthesis [36].

Minimizing the use of the combinations lower leg muscles is an objective to avoid signal collection from residual muscles. It can make the prosthesis more flexible to the variations in the condition of the amputation. SOL or MG with the addition of 1-2 upper limb muscles can form satisfactory combinations for moment estimations. However, position estimations require at least 2 lower limb muscles. The ranking of the performances can change with the initial weights of model training or due to the variances in training/test data set distribution. Therefore, a single muscle combination is not put forward. Instead, there are various combinations with above-threshold accuracy which can be considered further.

Although the aforementioned muscles' EMG signals are more effective overall, the contributions of each muscle are more evenly distributed in moment prediction. However, some muscles take a step forward overshadowing others in ankle position prediction. TA plays a key role in the prediction of position values.

Although there are several input combinations that consist of only upper leg muscles for moment estimation, position estimation results do not promise a successful choice. From the observations for the data set used, it can be said that sensory input from the lower leg is necessary for higher accuracy for ankle joint behavior estimation during stair climbing.

It should be noted that the data set used in this study consists of single subjects' gait measurements. Most of the available data presents between-subject average profiles including the data set of Keles and Yucesoy [106, 107]. There are few databases providing single subject data, but they do not include EMG measurements [2, 108].

4.1 Future Works

The data of Lencioni et al. was collected from able-bodied subjects. However, the controller is aimed to be designed for amputee people. According to the literature, there are significant differences between the biomechanics of the lower extremities of healthy and amputee people [12, 14]. On the other hand, the performance of the control algorithm may not be strongly dependent on the amputation level on the subject, but the user's learning capability to control the prosthesis by practice [109]. Additionally, available databases mostly do not provide stair climbing data [2]. An apparent complementary work to this study is the validation of the models with the gait data collected from the people with transtibial amputation. If required, the models can be trained with this data or improved by other methodologies. After that, other locomotion tasks can be focused to widen the scope of study.

This study uses and presents a systematic and generalized to some extent methodology for development of artificial neural network models for the prediction of human joint behaviour. Although model performances were optimized using several techniques, further optimization can be performed, e.g. hyperparameter optimization. Even if the main goal is to use only sEMG sensors, other sensor types can be introduced to the system. The amount of input-output relations may vary by using different data sets of other subjects or locomotion tasks. Therefore, the ideal model parameters and input sets may change. Trials with other data sets would be beneficial for validation of the proposed models.

The results show that it is possible to develop a controller for a powered ankle prosthesis being used in stair ambulation which is not a general scope of research. Furthermore, the use of only sEMG sensors provides satisfactory results as a preliminary study. A high-level control structure consisting of low-level control algorithms for various locomotion tasks and different outputs can be developed as a complementary work. Although the main purpose is to develop control algorithms for a powered ankle prosthesis, the studies on other assistive devices such as robotic lower limb exoskeletons can also benefit from this study. Further studies combining the controller with a commercially available powered ankle prosthesis can demonstrate the performance of the controller in real world applications. Moreover, possible challenges regarding the real world environment can be assessed. With the advancements of the stepwise work plan, design, development and manufacturing of a powered ankle prosthesis can be aimed as an ultimate purpose.

APPENDIX A. FEATURE EXTRACTION

A.1 Feature Definitions

Table A.1

The equations for some common time-domain features investigated in this study.

Feature	Definition
Integrated EMG	$IEMG = \sum_{n=1}^N x_n$
Mean Absolute Value	$MAV = \frac{1}{N} \sum_{n=1}^N x_n$
Modified Mean Absolute Value	$MMAV1 = \frac{1}{N} \sum_{n=1}^N w_n x_n$
Waveform Length	$WL = \sum_{n=1}^{N-1} x_{n+1} - x_n $
Willison's Amplitude	$WAMP = \sum_{n=1}^{N-1} f(x_n - x_{n+1})$
Mean Absolute Value Slope	$MAVS_i = MAV_{i+1} - MAV_i \quad ; \quad i = 1, 2, \dots, I - 1$
Root Mean Square	$RMS = \sqrt{\frac{1}{N} \sum_{n=1}^N x_n^2}$
Variance	$VAR = \frac{1}{N-1} \sum_{n=1}^N x_n^2$
Zero Crossing	$ZC = \sum_{n=1}^{N-1} [f(x_n \times x_{n+1}) \cap x_n - x_{n+1}] \geq threshold]$
Slope Sign Change	$SSC = \sum_{n=2}^{N-1} [f[(x_n - x_{n-1}) \times (x_n - x_{n+1})]]$ $f(x) = \begin{cases} 1 & x \geq threshold \\ 0 & otherwise \end{cases}$

A.2 Feature Performances

Table A.2: The results of feature selection study.

Feature Set	ρ	RMSE
MAV, WAMP, RMS	0.9477	0.0786
WL, IEMG, RMS	0.9471	0.0788
WL, IEMG, RMS, VAR	0.9458	0.0818
WL, MMAV1, RMS, VAR	0.9446	0.0810
WL, MMAV1, IEMG, RMS, VAR	0.9446	0.0804
IEMG, RMS, VAR	0.9444	0.0822
MAV, WL, MMAV1, IEMG, RMS	0.9439	0.0802
WL, MMAV1, IEMG, RMS	0.9427	0.0767
MAV, MMAV1, IEMG, RMS	0.9426	0.0816
WL, IEMG, VAR	0.9421	0.0801
MAV, WL, MMAV1, RMS, VAR	0.9411	0.0812
MAV, RMS, VAR	0.9409	0.0889
MAV, WL, IEMG, RMS, VAR	0.9408	0.0796
MAV, WL, IEMG, RMS	0.9394	0.0828
MAV, WL, MMAV1, RMS	0.9391	0.0867
MAV, MMAV1, IEMG	0.9385	0.0832
WL, RMS, VAR	0.9383	0.0820
MAV, SSC, WL, WAMP, MMAV1, VAR	0.9379	0.0942
MAV, WL, IEMG, VAR	0.9379	0.0882
MMAV1, IEMG, RMS	0.9378	0.0855
MAV, WL, MMAV1	0.9375	0.0838
MAV, IEMG, VAR	0.9375	0.0840
MAV, RMS	0.9373	0.0856
WL, MMAV1, RMS	0.9372	0.0812
MAV, WL	0.9371	0.0826
WL, MMAV1, IEMG, VAR	0.9370	0.0829
MAV, IEMG, RMS, VAR	0.9367	0.0848
MMAV1, IEMG, RMS, VAR	0.9364	0.0903
WL, IEMG	0.9363	0.0821
MAV, WL, WAMP, RMS	0.9361	0.0867
MAV, SSC, WL, WAMP, IEMG, VAR	0.9359	0.0927
MAV, WL, MMAV1, IEMG, VAR	0.9358	0.0830
MAV, WL, RMS, VAR	0.9356	0.0816

Table A.2 continued from previous page

Feature set	ρ	RMSE (mean)
MAV, WL, VAR	0.9353	0.0800
MAV, WL, IEMG	0.9353	0.0824
MAV, SSC, WAMP, MMAV1, VAR	0.9352	0.1000
WAMP, MMAV1, RMS, VAR	0.9349	0.0941
MMAV1, RMS	0.9348	0.0827
MAV, IEMG, RMS	0.9346	0.0812
SSC, WL, WAMP, MMAV1, IEMG, VAR	0.9343	0.1024
MAV, MMAV1, IEMG, VAR	0.9342	0.0843
MAV, SSC, WL, WAMP, MMAV1, IEMG, VAR	0.9337	0.1043
IEMG, RMS	0.9333	0.0862
MAV, WL, RMS	0.9332	0.0984
MAV, IEMG	0.9332	0.0816
WL, MMAV1, IEMG	0.9328	0.0812
MAV, SSC, RMS	0.9327	0.0976
RMS	0.9316	0.1031
IEMG, VAR	0.9315	0.0863
WAMP, RMS, VAR	0.9313	0.0958
MAV, MMAV1, VAR	0.9312	0.0850
WAMP, IEMG, RMS	0.9308	0.0921
MAV, SSC, WL, MMAV1, IEMG, RMS	0.9306	0.0942
MAV, SSC, WL, WAMP, MMAV1, IEMG, RMS, VAR	0.9305	0.0983
MAV, SSC, WL, WAMP, IEMG, RMS, VAR	0.9305	0.1024
SSC, WAMP, IEMG	0.9305	0.1052
WAMP, MMAV1, RMS	0.9303	0.0989

APPENDIX B. DETAILED TEST RESULTS FOR EACH OUTPUT

B.1 Stair Ascending Position

Table B.1: Stair ascending position estimation results with accuracy greater than 0.89.

Muscle set	ρ	RMSE
TA, SOL, MG, PL, BF, GM	0.9114	2.6080 \pm 1.3211
TA, SOL, MG, PL, RF, BF, GM	0.9101	2.6180 \pm 1.2905
TA, SOL, PL, BF	0.9078	2.5956 \pm 1.3406
TA, PL, RF, BF, GM	0.9068	2.5522 \pm 1.2182
TA, SOL, PL, RF, BF	0.9051	2.7053 \pm 1.3573
TA, SOL, MG, GM	0.9050	2.5892 \pm 1.3873
TA, MG, PL, BF	0.9049	2.5763 \pm 1.3507
TA, SOL, MG, PL, RF, GM	0.9038	2.5756 \pm 1.3079
TA, MG, BF, GM	0.9037	2.6553 \pm 1.4698
TA, SOL, MG, PL, RF	0.9028	2.5771 \pm 1.3475
TA, SOL, MG	0.9027	2.6108 \pm 1.3724
TA, SOL, MG, RF, BF, GM	0.9015	2.6062 \pm 1.3843
TA, SOL, PL, GM	0.9014	2.6578 \pm 1.3573
TA, SOL, MG, PL, VM, BF, GM	0.9012	2.6269 \pm 1.4471
TA, SOL, PL, RF, BF, GM	0.9010	2.5517 \pm 1.3053
TA, SOL, PL, RF	0.9002	2.5878 \pm 1.3170
TA, MG, RF, BF	0.8992	2.6646 \pm 1.3586
SOL, MG, PL, RF, BF	0.8992	2.6766 \pm 1.3473
TA, SOL, MG, RF, VM	0.8992	2.6041 \pm 1.3989
TA, MG, RF, VM, BF, GM	0.8990	2.6536 \pm 1.4090
TA, SOL, PL, RF, VM, BF	0.8986	2.6615 \pm 1.3399
SOL, MG, BF, GM	0.8982	2.6537 \pm 1.3997
TA, SOL, MG, RF, VM, GM	0.8982	2.6793 \pm 1.4105
SOL, MG, PL, RF, BF, GM	0.8982	2.6655 \pm 1.2927
TA, SOL, MG, VM, GM	0.8980	2.5821 \pm 1.3635
SOL, VM, BF, GM	0.8975	2.6438 \pm 1.3546

Table B.1 continued from previous page

Muscle set	ρ	RMSE
TA, SOL, MG, VM	0.8974	2.6218 \pm 1.3384
TA, SOL, MG, BF	0.8963	2.6550 \pm 1.4300
TA, SOL, MG, PL, VM, BF	0.8960	2.6763 \pm 1.4538
TA, SOL, MG, PL, RF, VM, BF, GM	0.8956	2.6735 \pm 1.4020
SOL, PL, RF, BF, GM	0.8955	2.6180 \pm 1.3377
SOL, PL, GM	0.8954	2.6239 \pm 1.3282
MG, BF, GM	0.8954	2.5983 \pm 1.3459
SOL, MG, RF, GM	0.8954	2.6940 \pm 1.3496
TA, SOL, BF	0.8953	2.5662 \pm 1.3131
TA, MG, PL, RF, BF, GM	0.8953	2.6763 \pm 1.3041
TA, PL, RF, BF	0.8950	2.6055 \pm 1.3720
TA, MG	0.8948	2.6068 \pm 1.3575
SOL, MG, PL, VM, BF	0.8947	2.6207 \pm 1.3580
TA, PL, BF, GM	0.8945	2.5807 \pm 1.3251
SOL, PL, VM, BF, GM	0.8945	2.5636 \pm 1.3187
TA, MG, RF	0.8943	2.5474 \pm 1.2866
TA, MG, RF, GM	0.8943	2.5987 \pm 1.3130
TA, SOL, MG, VM, BF	0.8943	2.6308 \pm 1.3676
TA, SOL, PL	0.8942	2.6823 \pm 1.3695
TA, MG, PL	0.8941	2.5442 \pm 1.3056
MG, PL, RF, VM, BF, GM	0.8941	2.6391 \pm 1.2631
TA, SOL, MG, PL, VM	0.8936	2.6394 \pm 1.2528
TA, MG, PL, VM, GM	0.8934	2.6350 \pm 1.2841
TA, SOL, PL, BF, GM	0.8931	2.6682 \pm 1.3335
TA, SOL, BF, GM	0.8929	2.5772 \pm 1.3717
TA, SOL, RF, BF	0.8927	2.7250 \pm 1.3796
SOL, PL, RF, GM	0.8927	2.6341 \pm 1.3338
SOL, PL, BF	0.8923	2.6607 \pm 1.3287
MG, PL, RF, BF	0.8923	2.6459 \pm 1.2999
SOL, PL, VM, BF	0.8922	2.5581 \pm 1.3019
SOL, MG, RF, BF, GM	0.8922	2.6923 \pm 1.3636
TA, SOL, MG, PL	0.8921	2.6980 \pm 1.4394
TA, SOL, PL, VM, BF	0.8921	2.6792 \pm 1.4103
TA, MG, BF	0.8920	2.5838 \pm 1.3875
TA, SOL, MG, PL, GM	0.8916	2.6846 \pm 1.4463

Table B.1 continued from previous page

Muscle set	ρ	RMSE
SOL, MG, RF, VM, BF, GM	0.8916	2.6129 \pm 1.2958
TA, SOL, PL, RF, VM, BF, GM	0.8915	2.5916 \pm 1.2670
TA, SOL	0.8914	2.6266 \pm 1.3645
TA, MG, PL, RF, GM	0.8914	2.6457 \pm 1.3517
TA, MG, VM, BF, GM	0.8913	2.5800 \pm 1.2825
TA, MG, RF, BF, GM	0.8913	2.6454 \pm 1.3806
TA, PL, GM	0.8911	2.5836 \pm 1.2377
MG, PL, GM	0.8910	2.6908 \pm 1.2510
TA, SOL, MG, PL, RF, VM, GM	0.8910	2.5946 \pm 1.3552
TA, SOL, PL, VM, GM	0.8909	2.7514 \pm 1.3492
TA, MG, PL, VM, BF, GM	0.8907	2.6303 \pm 1.3064
TA, SOL, RF, VM, BF	0.8904	2.6003 \pm 1.3369
TA, SOL, MG, PL, RF, VM, BF	0.8904	2.5647 \pm 1.2747

B.2 Stair Ascending Moment

Table B.2: Stair ascending moment estimation results, the 100 best-performing input set.

Muscle set	ρ	RMSE
SOL, MG, RF, VM, BF, GM	0.9365	0.0872 \pm 0.0533
TA, MG, PL, RF, GM	0.9348	0.0883 \pm 0.0508
TA, MG, RF, VM	0.9335	0.0876 \pm 0.0468
TA, MG, PL, RF, VM, GM	0.9332	0.0930 \pm 0.0482
TA, SOL, MG, RF	0.9326	0.0865 \pm 0.0481
TA, SOL, VM	0.9324	0.0911 \pm 0.0499
SOL, MG, GM	0.9324	0.0922 \pm 0.0564
SOL, MG, RF	0.9323	0.0868 \pm 0.0514
TA, SOL, MG, PL, VM	0.9320	0.0904 \pm 0.0542
SOL, MG, PL, RF, VM, GM	0.9316	0.0860 \pm 0.0511
MG, PL, VM	0.9314	0.0911 \pm 0.0526
SOL, MG, VM	0.9312	0.0895 \pm 0.0547
SOL, MG, PL, VM, GM	0.9308	0.0872 \pm 0.0522
MG, PL, RF, VM	0.9303	0.0894 \pm 0.0508

Table B.2 continued from previous page

Muscle set	ρ	RMSE
TA, MG, VM, BF, GM	0.9301	0.0888 \pm 0.0503
TA, SOL, MG, RF, VM	0.9301	0.0885 \pm 0.0529
SOL, MG, PL, RF	0.9300	0.0867 \pm 0.0510
TA, MG, VM, GM	0.9298	0.0933 \pm 0.0557
MG, RF, VM	0.9296	0.0877 \pm 0.0514
SOL, RF	0.9292	0.0912 \pm 0.0507
TA, SOL, PL, RF, VM, BF	0.9289	0.0870 \pm 0.0471
TA, SOL, MG, RF, VM, BF, GM	0.9288	0.0864 \pm 0.0482
SOL, MG, PL, RF, VM	0.9286	0.0894 \pm 0.0533
MG, RF, BF	0.9285	0.0908 \pm 0.0534
TA, SOL, VM, GM	0.9283	0.0921 \pm 0.0508
SOL, MG, RF, VM, GM	0.9281	0.0927 \pm 0.0542
TA, SOL, MG, RF, VM, GM	0.9281	0.0913 \pm 0.0498
TA, MG, PL, VM, BF	0.9280	0.0916 \pm 0.0553
MG, PL, VM, BF	0.9278	0.0921 \pm 0.0559
SOL, VM, GM	0.9278	0.0907 \pm 0.0546
MG, PL, RF	0.9276	0.0933 \pm 0.0535
SOL, MG, PL, VM, BF	0.9275	0.0909 \pm 0.0546
TA, MG, VM	0.9274	0.0905 \pm 0.0522
SOL, RF, VM	0.9274	0.0886 \pm 0.0535
MG, RF	0.9273	0.0881 \pm 0.0523
TA, SOL, PL	0.9272	0.0876 \pm 0.0483
SOL, PL, VM, GM	0.9271	0.0941 \pm 0.0562
MG, RF, GM	0.9270	0.0904 \pm 0.0529
SOL, PL, RF, GM	0.9268	0.0900 \pm 0.0510
TA, MG, PL, VM, BF, GM	0.9267	0.0909 \pm 0.0516
MG, PL, RF, GM	0.9266	0.0925 \pm 0.0514
SOL, MG, PL, BF	0.9264	0.0934 \pm 0.0562
SOL, MG, VM, BF	0.9263	0.0919 \pm 0.0564
SOL, PL, GM	0.9263	0.0895 \pm 0.0515
TA, MG, RF, VM, BF, GM	0.9261	0.0870 \pm 0.0492
TA, SOL, MG, PL, RF	0.9261	0.0906 \pm 0.0526
SOL, PL, VM, BF, GM	0.9260	0.0908 \pm 0.0535
SOL, RF, BF	0.9260	0.0898 \pm 0.0506
TA, MG, PL, VM	0.9257	0.0896 \pm 0.0494

Table B.2 continued from previous page

Muscle set	ρ	RMSE
TA, SOL, PL, VM, GM	0.9257	0.0904 \pm 0.0480
SOL, MG, PL, RF, GM	0.9257	0.0870 \pm 0.0483
MG, PL, RF, BF, GM	0.9255	0.0921 \pm 0.0531
TA, SOL, PL, BF	0.9252	0.0941 \pm 0.0541
SOL, RF, BF, GM	0.9251	0.0894 \pm 0.0524
TA, SOL, MG, GM	0.9249	0.0916 \pm 0.0470
TA, MG, PL, RF	0.9249	0.0878 \pm 0.0472
TA, SOL, MG	0.9248	0.0912 \pm 0.0498
TA, MG, PL, RF, BF, GM	0.9247	0.0862 \pm 0.0481
MG, PL, VM, BF, GM	0.9247	0.0926 \pm 0.0552
SOL, MG	0.9247	0.0909 \pm 0.0540
SOL, RF, VM, GM	0.9247	0.0885 \pm 0.0528
SOL, MG, RF, VM	0.9247	0.0896 \pm 0.0497
TA, RF, VM, GM	0.9246	0.0975 \pm 0.0547
MG, RF, VM, BF	0.9246	0.0914 \pm 0.0539
TA, SOL, MG, PL, BF	0.9245	0.0883 \pm 0.0502
MG, PL, RF, VM, BF, GM	0.9244	0.0905 \pm 0.0553
MG, RF, BF, GM	0.9242	0.0887 \pm 0.0546
MG, VM, BF, GM	0.9240	0.0918 \pm 0.0569
TA, SOL, MG, VM, BF, GM	0.9239	0.0922 \pm 0.0507
SOL, MG, PL, RF, BF, GM	0.9239	0.0898 \pm 0.0472
SOL, PL, RF, VM, BF	0.9238	0.0905 \pm 0.0539
TA, SOL, MG, PL, RF, VM, GM	0.9237	0.0896 \pm 0.0522
TA, SOL, RF, BF	0.9235	0.0917 \pm 0.0524
SOL, RF, VM, BF, GM	0.9233	0.0921 \pm 0.0565
MG, PL, RF, VM, BF	0.9232	0.0898 \pm 0.0493
TA, SOL, MG, PL	0.9231	0.0900 \pm 0.0465
SOL, MG, PL	0.9231	0.0945 \pm 0.0575
TA, MG, RF, GM	0.9229	0.0884 \pm 0.0502
TA, SOL, PL, RF, VM	0.9229	0.0893 \pm 0.0484
TA, MG, VM, BF	0.9229	0.0943 \pm 0.0526
TA, SOL, RF, GM	0.9228	0.0882 \pm 0.0464
TA, PL, VM	0.9227	0.0934 \pm 0.0509
SOL, MG, PL, BF, GM	0.9226	0.0902 \pm 0.0525
TA, SOL, MG, PL, VM, GM	0.9226	0.0893 \pm 0.0511

Table B.2 continued from previous page

Muscle set	ρ	RMSE
TA, MG, RF, VM, GM	0.9226	0.0906 \pm 0.0509
SOL, RF, VM, BF	0.9225	0.0903 \pm 0.0598
TA, MG, RF, BF	0.9225	0.0924 \pm 0.0507
SOL, MG, RF, BF	0.9223	0.0873 \pm 0.0520
MG, VM	0.9223	0.0907 \pm 0.0515
SOL, PL, RF, VM, GM	0.9223	0.0963 \pm 0.0569
SOL, PL, RF, VM	0.9220	0.0910 \pm 0.0567
SOL, PL, BF, GM	0.9217	0.0969 \pm 0.0553
TA, SOL, PL, RF, VM, GM	0.9217	0.0922 \pm 0.0527
TA, SOL, MG, PL, RF, VM, BF, GM	0.9217	0.0901 \pm 0.0527
TA, SOL, MG, PL, RF, BF	0.9216	0.0894 \pm 0.0499
SOL, MG, PL, VM	0.9215	0.0927 \pm 0.0547
SOL, MG, VM, GM	0.9215	0.0946 \pm 0.0586
SOL, GM	0.9215	0.0910 \pm 0.0519
TA, SOL, MG, PL, VM, BF	0.9215	0.0895 \pm 0.0484
TA, MG, PL, RF, VM	0.9214	0.0920 \pm 0.0518
PL, GM	0.9214	0.0948 \pm 0.0538

B.3 Stair Descending Position

Table B.3: Stair descending position estimation results with accuracy greater than 0.89.

Muscle set	ρ	RMSE
TA, SOL, MG, RF, VM	0.9126	2.6953 \pm 1.2551
TA, MG, PL, RF, BF	0.9124	2.4872 \pm 1.2276
TA, MG, RF, VM, BF	0.9117	2.8456 \pm 1.1641
TA, MG, PL, RF	0.9103	2.8267 \pm 1.2728
TA, MG, BF	0.9102	3.0119 \pm 1.1593
TA, SOL, PL, RF, VM, GM	0.9098	2.9346 \pm 1.1984
TA, MG, VM, BF, GM	0.9091	2.9440 \pm 1.2013
TA, MG, VM	0.9083	3.0205 \pm 1.2073
TA, SOL, PL	0.9075	3.0600 \pm 1.3524
TA, SOL, MG, VM, GM	0.9075	3.0691 \pm 1.1228

Table B.3 continued from previous page

Muscle set	ρ	RMSE
TA, SOL, MG, RF, VM, BF	0.9071	2.9296 \pm 0.9954
TA, SOL, PL, RF, VM, BF	0.9065	2.9543 \pm 1.0907
TA, PL, RF	0.9059	2.9924 \pm 1.0858
TA, MG, RF	0.9057	3.0650 \pm 1.1314
TA, MG, PL, VM	0.9055	2.9171 \pm 1.2732
TA, MG, PL, BF, GM	0.9042	2.8126 \pm 1.0478
TA, RF, VM, BF, GM	0.9036	2.9499 \pm 0.9191
TA, MG, PL, VM, BF	0.9036	2.8373 \pm 1.1226
TA, PL	0.9035	2.9562 \pm 1.2874
TA, MG, RF, GM	0.9029	2.9579 \pm 1.0320
TA, MG	0.9027	3.3542 \pm 1.0458
TA, SOL, PL, VM	0.9023	3.0094 \pm 1.2909
TA, SOL, MG, PL, RF, BF	0.9019	2.7601 \pm 1.3837
TA, MG, RF, VM, BF, GM	0.9012	2.6184 \pm 1.0612
TA, SOL, RF, BF, GM	0.9012	3.0295 \pm 1.0974
TA, MG, PL	0.9011	3.0324 \pm 1.3726
TA, SOL, PL, RF, BF	0.9003	2.6960 \pm 1.4263
TA, RF, VM, BF	0.8998	2.8569 \pm 1.0511
TA, SOL, RF, VM, BF	0.8998	2.9177 \pm 1.2298
MG, VM, BF	0.8996	2.6231 \pm 1.3871
TA, BF, GM	0.8985	3.1244 \pm 1.1070
TA, PL, RF, BF, GM	0.8983	2.7249 \pm 1.3455
MG, RF, VM, BF	0.8979	2.9925 \pm 1.1047
TA, MG, VM, GM	0.8979	2.9859 \pm 0.8162
TA, SOL, VM, BF	0.8977	3.0897 \pm 1.1286
TA, MG, RF, BF	0.8976	3.2549 \pm 1.0948
TA, MG, RF, VM	0.8973	2.7091 \pm 1.2338
TA, MG, BF, GM	0.8971	2.8838 \pm 1.1863
TA, PL, RF, VM, BF, GM	0.8971	3.1089 \pm 1.0693
TA, MG, VM, BF	0.8970	2.7889 \pm 1.3570
TA, VM, BF	0.8970	2.8624 \pm 1.1875
MG, BF	0.8969	2.9639 \pm 1.2641
MG, PL, VM, BF	0.8969	2.6761 \pm 1.2628
TA, PL, RF, VM, GM	0.8963	2.9123 \pm 1.0934
BF, GM	0.8963	3.0700 \pm 1.1269

Table B.3 continued from previous page

Muscle set	ρ	RMSE
TA, RF	0.8961	3.2128 \pm 1.2328
TA, RF, BF	0.8959	3.0444 \pm 1.1740
TA, SOL, MG, PL, VM	0.8958	3.0465 \pm 1.1189
TA, PL, GM	0.8955	3.2706 \pm 1.0368
TA, SOL, MG, PL, BF, GM	0.8953	2.7451 \pm 1.2572
TA, RF, VM, GM	0.8952	2.8639 \pm 1.3405
PL, VM, BF	0.8951	2.8822 \pm 1.3001
TA, MG, PL, RF, VM, BF	0.8948	2.7071 \pm 1.4021
TA, PL, RF, VM, BF	0.8944	2.7171 \pm 1.1923
TA, PL, VM, GM	0.8944	3.1350 \pm 1.0623
TA, SOL, VM, GM	0.8943	2.9415 \pm 1.3257
TA, MG, PL, GM	0.8937	3.1676 \pm 1.1457
TA, RF, VM	0.8935	3.2011 \pm 0.9741
MG, PL, GM	0.8935	3.1062 \pm 1.1827
TA, PL, VM, BF, GM	0.8935	2.9731 \pm 1.4603
TA, SOL, PL, BF	0.8933	3.1518 \pm 1.2523
TA, SOL, RF	0.8931	3.3521 \pm 1.1247
TA, MG, RF, BF, GM	0.8930	2.7179 \pm 1.0718
TA, SOL	0.8924	3.3331 \pm 1.3718
MG, GM	0.8922	3.1574 \pm 1.1553
TA, SOL, PL, RF, GM	0.8920	3.1655 \pm 1.1350
TA, RF, BF, GM	0.8916	2.7946 \pm 1.1151
TA, MG, PL, RF, VM	0.8915	2.9670 \pm 1.3066
TA, SOL, GM	0.8913	3.4376 \pm 1.1013
TA, SOL, MG, RF, GM	0.8913	3.0813 \pm 1.1126
TA, SOL, BF	0.8913	3.2689 \pm 1.1939
PL, BF, GM	0.8909	3.0592 \pm 1.0762
TA, SOL, PL, BF, GM	0.8909	3.1176 \pm 1.0523
TA, SOL, MG	0.8909	3.2178 \pm 1.2631
TA, SOL, PL, VM, BF	0.8907	2.9390 \pm 1.2770
TA, SOL, MG, VM	0.8905	2.8886 \pm 1.2785
MG, PL, BF	0.8900	3.1762 \pm 1.2239

B.4 Stair Descending Moment

Table B.4: Stair descending moment estimation results, the 100 best-performing input set.

Muscle set	ρ	RMSE
MG, RF, BF	0.9324	0.1169 \pm 0.0701
TA, MG, VM	0.9296	0.1176 \pm 0.0711
TA, MG, PL, RF, VM, BF	0.9289	0.1214 \pm 0.0698
TA, SOL, MG, VM, BF	0.9263	0.1199 \pm 0.0691
MG, VM	0.9260	0.1188 \pm 0.0700
MG, BF, GM	0.9250	0.1189 \pm 0.0692
TA, MG	0.9239	0.1196 \pm 0.0702
MG, BF	0.9237	0.1165 \pm 0.0698
SOL, VM	0.9236	0.1202 \pm 0.0693
TA, MG, RF	0.9235	0.1173 \pm 0.0661
TA, SOL, MG, RF	0.9235	0.1170 \pm 0.0720
TA, MG, PL, RF	0.9232	0.1165 \pm 0.0655
SOL, MG, PL, RF, BF	0.9232	0.1232 \pm 0.0755
TA, SOL, MG	0.9228	0.1184 \pm 0.0708
SOL, MG, RF, VM, BF	0.9228	0.1204 \pm 0.0740
MG, RF	0.9225	0.1200 \pm 0.0713
TA, SOL, RF	0.9224	0.1174 \pm 0.0690
TA, MG, RF, BF	0.9221	0.1172 \pm 0.0679
MG, PL, BF, GM	0.9221	0.1198 \pm 0.0719
TA, SOL, MG, PL, VM	0.9220	0.1205 \pm 0.0721
MG, RF, BF, GM	0.9219	0.1162 \pm 0.0699
TA, SOL, MG, RF, VM, GM	0.9213	0.1186 \pm 0.0668
MG	0.9209	0.1200 \pm 0.0732
MG, GM	0.9208	0.1153 \pm 0.0716
MG, PL, BF	0.9206	0.1189 \pm 0.0710
MG, PL, RF, GM	0.9201	0.1207 \pm 0.0712
MG, PL, GM	0.9198	0.1184 \pm 0.0723
TA, MG, PL	0.9194	0.1146 \pm 0.0662
TA, SOL, MG, PL, BF	0.9193	0.1202 \pm 0.0691
MG, PL, RF, VM, BF	0.9193	0.1233 \pm 0.0741
TA, SOL, VM, GM	0.9191	0.1221 \pm 0.0712
TA, SOL, VM, BF	0.9190	0.1209 \pm 0.0691

Table B.4 continued from previous page

Muscle set	ρ	RMSE
SOL, MG, BF, GM	0.9189	0.1183 \pm 0.0753
SOL, RF, BF, GM	0.9189	0.1225 \pm 0.0720
TA, MG, RF, GM	0.9189	0.1161 \pm 0.0694
TA, SOL, PL, GM	0.9187	0.1229 \pm 0.0713
TA, MG, VM, BF, GM	0.9187	0.1204 \pm 0.0687
TA, SOL, MG, PL, RF, VM	0.9187	0.1191 \pm 0.0697
SOL, VM, BF, GM	0.9187	0.1217 \pm 0.0752
MG, PL, VM, BF, GM	0.9186	0.1238 \pm 0.0701
TA, VM	0.9183	0.1258 \pm 0.0730
TA, MG, PL, VM	0.9183	0.1250 \pm 0.0691
TA, MG, RF, VM, BF	0.9182	0.1196 \pm 0.0695
MG, PL, RF, BF	0.9179	0.1220 \pm 0.0730
SOL, MG, VM, BF, GM	0.9177	0.1217 \pm 0.0758
MG, PL, VM, GM	0.9172	0.1208 \pm 0.0746
TA, MG, RF, VM, BF, GM	0.9172	0.1190 \pm 0.0670
TA, SOL, MG, VM	0.9171	0.1211 \pm 0.0674
TA, MG, VM, GM	0.9168	0.1246 \pm 0.0665
TA, SOL, MG, VM, GM	0.9167	0.1179 \pm 0.0683
TA, SOL, MG, PL, RF	0.9167	0.1205 \pm 0.0640
TA, SOL, MG, PL, RF, BF	0.9166	0.1193 \pm 0.0696
TA, MG, BF, GM	0.9166	0.1212 \pm 0.0691
SOL, MG, VM, BF	0.9166	0.1196 \pm 0.0709
TA, MG, PL, VM, BF	0.9164	0.1236 \pm 0.0697
TA, SOL, VM, BF, GM	0.9163	0.1220 \pm 0.0736
TA, SOL, VM	0.9161	0.1183 \pm 0.0704
TA, MG, VM, BF	0.9160	0.1203 \pm 0.0681
SOL, MG, RF, BF	0.9158	0.1173 \pm 0.0703
TA, SOL, MG, RF, VM	0.9158	0.1207 \pm 0.0648
TA, SOL, PL, RF	0.9155	0.1180 \pm 0.0684
SOL, GM	0.9154	0.1188 \pm 0.0715
TA, MG, PL, GM	0.9153	0.1185 \pm 0.0696
SOL, BF, GM	0.9153	0.1222 \pm 0.0737
PL	0.9152	0.1227 \pm 0.0710
SOL, VM, GM	0.9151	0.1213 \pm 0.0737
SOL, MG, BF	0.9151	0.1192 \pm 0.0728

Table B.4 continued from previous page

Muscle set	ρ	RMSE
TA, MG, PL, RF, BF, GM	0.9150	0.1218 \pm 0.0695
MG, RF, VM	0.9148	0.1243 \pm 0.0717
SOL, VM, BF	0.9148	0.1218 \pm 0.0720
MG, PL	0.9147	0.1213 \pm 0.0690
MG, VM, BF, GM	0.9145	0.1226 \pm 0.0732
BF	0.9144	0.1264 \pm 0.0717
SOL, MG	0.9142	0.1217 \pm 0.0726
PL, VM, BF	0.9142	0.1278 \pm 0.0730
TA, SOL, MG, VM, BF, GM	0.9141	0.1157 \pm 0.0678
VM, BF, GM	0.9138	0.1266 \pm 0.0764
RF	0.9137	0.1233 \pm 0.0740
SOL, PL, RF, BF, GM	0.9136	0.1214 \pm 0.0733
TA, SOL, PL	0.9136	0.1179 \pm 0.0658
TA, BF, GM	0.9135	0.1281 \pm 0.0774
SOL, MG, RF, GM	0.9134	0.1156 \pm 0.0713
TA, PL, RF, GM	0.9134	0.1257 \pm 0.0733
MG, VM, GM	0.9133	0.1229 \pm 0.0734
MG, RF, VM, BF	0.9132	0.1197 \pm 0.0723
PL, GM	0.9130	0.1245 \pm 0.0718
MG, PL, RF, BF, GM	0.9123	0.1231 \pm 0.0733
SOL, MG, RF, VM, BF, GM	0.9123	0.1204 \pm 0.0724
SOL, PL, VM, BF	0.9123	0.1265 \pm 0.0741
SOL	0.9122	0.1194 \pm 0.0686
TA, MG, PL, BF	0.9121	0.1178 \pm 0.0670
MG, PL, VM, BF	0.9117	0.1212 \pm 0.0708
SOL, MG, PL, RF, VM, BF	0.9116	0.1237 \pm 0.0728
SOL, MG, VM	0.9114	0.1225 \pm 0.0698
TA, SOL, RF, VM, BF	0.9113	0.1209 \pm 0.0709
PL, VM, GM	0.9113	0.1268 \pm 0.0731
TA, SOL, MG, PL, VM, GM	0.9111	0.1165 \pm 0.0680
TA, SOL, MG, BF	0.9110	0.1202 \pm 0.0705
TA, MG, PL, VM, BF, GM	0.9110	0.1224 \pm 0.0675
RF, VM, BF	0.9109	0.1269 \pm 0.0744

REFERENCES

1. Hellmers, S., S. Lau, R. Diekmann, *et al.*, “Evaluation of power-based stair climb performance via inertial measurement units,” *Biomedical Engineering Systems and Technologies*, pp. 238–261, 2019. https://doi.org/10.1007/978-3-030-29196-9_13.
2. Lencioni, T., I. Carpinella, M. Rabuffetti, *et al.*, “Human kinematic, kinetic and EMG data during different walking and stair ascending and descending tasks,” *Scientific Data*, Vol. 61, Dec 2019. <https://doi.org/10.1038/s41597-019-0323-z>.
3. Burdett, R. G., “Forces predicted at the ankle during running,” *Medicine and Science in Sports and Exercise*, Vol. 14, no. 4, pp. 308–316, 1982.
4. Shiming, Y., “The conceptual design of an ankle rehabilitation robot and research on its control strategy,” *Harbin Institute of Technology*, 2016.
5. Smith, D. G., and J. R. Fergason, “Transtibial amputations,” *Clinical Orthopaedics and Related Research*, Vol. 361, pp. 108–115, Apr 1999. doi: 10.1097/00003086-199904000-00015. PMID: 10212603.
6. Molina, C., and J. Faulk, “Lower extremity amputation,” *StatPearls[Internet]*, Sep 2020. PMID: 31536201.
7. Ziegler-Graham, K., E. J. MacKenzie, P. L. Ephraim, *et al.*, “Estimating the prevalence of limb loss in the United States: 2005 to 2050,” *Archives of Physical Medicine and Rehabilitation*, Vol. 89, no. 3, pp. 422–429, 2008. <https://doi.org/10.1016/j.apmr.2007.11.005>.
8. Reiber, G. E., E. J. Boyko, and D. G. Smith, “Lower extremity foot ulcers and amputation in diabetes,” *Diabetes in America*, Vol. 2, pp. 409–428, Jan 1995.
9. Schaffalitzky, E., P. Gallagher, M. Maclachlan, *et al.*, “Understanding the benefits of prosthetic prescription: Exploring the experiences of practitioners and lower limb prosthetic users,” *Disability and Rehabilitation*, Vol. 33, no. 15-16, pp. 1314–1323, 2011. <https://doi.org/10.3109/09638288.2010.529234>.
10. Windrich, M., M. Grimmer, O. Christ, *et al.*, “Active lower limb prosthetics: a systematic review of design issues and solutions,” *Biomedical engineering online*, Vol. 15, Dec 2016. <https://doi.org/10.1186/s12938-016-0284-9>.
11. Herr, H. M., and A. M. Grabowski, “Bionic ankle-foot prosthesis normalizes walking gait for persons with leg amputation,” *Proceedings of the Royal Society B: Biological Sciences*, Vol. 279, pp. 457–464, Jul 2011. <https://doi.org/10.1098/rspb.2011.1194>.
12. Waters, R. L., J. P. J. D. Antonelli, *et al.*, “Energy cost of walking of amputees: the influence of level of amputation,” *J Bone Joint Surg Am*, Vol. 58, pp. 42–46, Jan 1976. PMID: 1249111.
13. Varol, H. A., F. Sup, and M. Goldfarb, “Multiclass real-time intent recognition of a powered lower limb prosthesis,” *IEEE Transactions on Biomedical Engineering*, Vol. 57, pp. 542–551, Mar 2010. <https://doi.org/10.1109/tbme.2009.2034734>.
14. Grimmer, M., and A. Seyfarth, “Mimicking human-like leg function in prosthetic limbs,” in *Neuro-robotics: From Brain Machine Interfaces to Rehabilitation Robotics*, pp. 105–155, Berlin: Springer, Jul 2014.

15. Bellman, R. D., M. A. Holgate, and T. G. Sugar, “Sparky 3: Design of an active robotic ankle prosthesis with two actuated degrees of freedom using regenerative kinetics,” *2008 2nd IEEE RAS EMBS International Conference on Biomedical Robotics and Biomechanics*, 2008. <https://doi.org/10.1109/biorob.2008.4762887>.
16. Au, S. K., P. Dilworth, and H. Herr, “An ankle-foot emulation system for the study of human walking biomechanics,” *Proceedings 2006 IEEE International Conference on Robotics and Automation*, 2006. <https://doi.org/10.1109/robot.2006.1642148>.
17. Alleva, S., M. G. Antonelli, P. B. Zobel, *et al.*, “Biomechanical design and prototyping of a powered ankle-foot prosthesis,” *Materials*, Vol. 13, Dec 2020. <https://doi.org/10.3390/ma13245806>.
18. Cherelle, P., V. Grosu, A. Matthys, *et al.*, “Design and validation of the ankle mimicking prosthetic foot 2.0,” *IEEE Transactions on Neural Systems and Rehabilitation Engineering*, Vol. 22, pp. 138–148, Jan 2014. <https://doi.org/10.1109/tnsre.2013.2282416>.
19. Eslamy, M., F. Oswald, and A. F. Schilling, “Estimation of knee angles based on thigh motion: A functional approach and implications for high-level controlling of active prosthetic knees,” *IEEE Control Systems Magazine*, Vol. 40, pp. 49–61, Jun 2020. doi:10.1109/MCS.2020.2976384.
20. Dey, S., M. Eslamy, T. Yoshida, *et al.*, “A support vector regression approach for continuous prediction of ankle angle and moment during walking: An implication for developing a control strategy for active ankle prostheses,” *2019 IEEE 16th International Conference on Rehabilitation Robotics (ICORR)*, pp. 727–733, 2019. <https://doi.org/10.1109/icorr.2019.8779445>.
21. Jiang, X., M. Gholami, M. Khoshnam, *et al.*, “Estimation of ankle joint power during walking using two inertial sensors,” *Sensors*, Vol. 19, Jun 2019. <https://doi.org/10.3390/s19122796>.
22. Mahdavian, M., S. Arzanpour, and E. J. Park, “Motion generation of a wearable hip exoskeleton robot using machine learning-based estimation of ground reaction forces and moments,” *2019 IEEE/ASME International Conference on Advanced Intelligent Mechatronics (AIM)*, pp. 796–801, 2019. <https://doi.org/10.1109/aim.2019.8868759>.
23. Xiong, B., N. N Zeng, H. Li, *et al.*, “Intelligent prediction of human lower extremity joint moment: An artificial neural network approach,” *IEEE Access*, Vol. 7, pp. 29973–29980, 2019. doi:10.1109/access.2019.2900591.
24. Shultz, A. H., B. E. Lawson, and M. Goldfarb, “Walking on uneven terrain with a powered ankle prosthesis: A preliminary assessment,” *2015 37th Annual International Conference of the IEEE Engineering in Medicine and Biology Society (EMBC)*, pp. 5299–5302, 2015. <https://doi.org/10.1109/embc.2015.7319587>.
25. Huang, H., T. A. Kuiken, and R. D. Lipschutz, “A strategy for identifying locomotion modes using surface electromyography,” *IEEE Transactions on Biomedical Engineering*, Vol. 56, pp. 65–73, Jan 2009. <https://doi.org/10.1109/tbme.2008.2003293>.
26. Dhir, N., “Kriging for prosthesis control,” in *Powered Prostheses: Design, Control, and Clinical Applications* (Dallali, H., E. Demircan, and M. Rastgaar, eds.), pp. 57–112, Academic Press, 2020. <https://doi.org/10.1016/b978-0-12-817450-0.00004-3>.

27. Lenzi, T., L. Hargrove, and J. Sensinger, "Speed-adaptation mechanism: Robotic prostheses can actively regulate joint torque," *IEEE Robotics Automation Magazine*, Vol. 21, pp. 94–107, Dec 2014. <https://doi.org/10.1109/mra.2014.2360305>.
28. Fleming, A., N. Stafford, S. Huang, *et al.*, "Myoelectric control of robotic lower limb prostheses: A review of electromyography interfaces, control paradigms, challenges and future directions," *Journal of Neural Engineering*, Vol. 18, no. 4, 2021. <https://doi.org/10.1088/1741-2552/ac1176>.
29. Ferreira, C., and R. Augusto, "Application of surface electromyography in the dynamics of human movement," in *Computational Intelligence in Electromyography Analysis - A Perspective on Current Applications and Future Challenges* (Naik, G. R., ed.), pp. 57–112, Academic Press, Oct 2012. <https://doi.org/10.5772/52463>.
30. Reaz, M. B., M. S. Hussain, and F. Mohd-Yasin, "Techniques of EMG signal analysis: Detection, processing, classification and applications," *Biological Procedures Online*, Vol. 8, pp. 11–35, Dec 2006. <https://doi.org/10.1251/bpo115>.
31. Pilkar, R., K. Momeni, A. Ramanujam, *et al.*, "Use of surface EMG in clinical rehabilitation of individuals with sci: Barriers and future considerations," *Frontiers in Neurology*, Vol. 11, p. 1680, Dec 2020. <https://doi.org/10.3389/fneur.2020.578559>.
32. Drost, G., D. F. Stegeman, B. G. van Engelen, *et al.*, "Clinical applications of high-density surface EMG: a systematic review," *Journal of Electromyography and Kinesiology*, Vol. 16, no. 6, pp. 586–602, 2006.
33. Su, C., S. Chen, H. Jiang, *et al.*, "Ankle joint torque prediction based on surface electromyographic and angular velocity signals," *IEEE Access*, Vol. 8, pp. 217681–217687, 2020. <https://doi.org/10.1109/access.2020.3040820>.
34. Ranz, E. C., J. M. Wilken, D. A. Gajewski, *et al.*, "The influence of limb alignment and transfemoral amputation technique on muscle capacity during gait," *Computer Methods in Biomechanics and Biomedical Engineering*, Vol. 20, pp. 1167–1174, Jun 2017. <https://doi.org/10.1080/10255842.2017.1340461>.
35. Robinson, V., K. Sansam, L. Hirst, *et al.*, "Major lower limb amputation - what, why and how to achieve the best results," *Orthopaedics and Trauma*, Vol. 24, no. 4, pp. 276–285, 2010. <https://doi.org/10.1016/j.mporth.2010.03.017>.
36. Au, S., M. Berniker, and H. Herr, "Powered ankle-foot prosthesis to assist level-ground and stair-descent gaits," *Neural Networks*, Vol. 21, pp. 654–666, May 2008. <https://doi.org/10.1016/j.neunet.2008.03.006>.
37. Nadeau, S., B. J. McFadyen, and F. Malouin, "Frontal and sagittal plane analyses of the stair climbing task in healthy adults aged over 40 years: what are the challenges compared to level walking?," *Clinical Biomechanics*, Vol. 18, pp. 950–959, Dec 2003. doi: 10.1016/s0268-0033(03)00179-7.
38. Silva, L. M., and N. Stergiou, "The basics of gait analysis," in *Biomechanics and Gait Analysis* (Stergiou, N., ed.), pp. 225–250, Academic Press, 2020. <https://doi.org/10.1016/b978-0-12-813372-9.00007-5>.
39. Laribi, M. A., and S. Zegloul, "Human lower limb operation tracking via motion capture systems," in *Design and Operation of Human Locomotion Systems* (Ceccarelli, M., and G. Carbone, eds.), pp. 83–107, Academic Press, 2020. <https://doi.org/10.1016/b978-0-12-815659-9.00004-4>.

40. Joseph, J., and R. Watson, "Telemetering electromyography of muscles used in walking up and down stairs," *J Bone Joint Surg*, Vol. 49, pp. 774–780, 1967.
41. Marshall, R. N., P. T. Morgan, E. Martinez-Valdes, *et al.*, "Quadriceps muscle electromyography activity during physical activities and resistance exercise modes in younger and older adults," *Experimental Gerontology*, Vol. 136, p. 110965, 2020. <https://doi.org/10.1016/j.exger.2020.110965>.
42. Farrag, A., and W. Elsayed, "Hip and knee sagittal angles and muscle activation in stair locomotion: Impact of age and gender," *Gait Posture*, Vol. 42, Sep 2015. <https://doi.org/10.1016/j.gaitpost.2015.06.124>.
43. Syczewska, M., M. Kalinowska, and E. Szczerbik, "Normative data of stair ascent for children and adolescents (kinematics and EMG)," *Gait Posture*, Vol. 30, Nov 2009. <https://doi.org/10.1016/j.gaitpost.2009.08.172>.
44. Lewis, J., G. Freisinger, X. Pan, *et al.*, "Changes in lower extremity peak angles, moments and muscle activations during stair climbing at different speeds," *Journal of Electromyography and Kinesiology*, Vol. 25, pp. 982–989, Dec 2015. <https://doi.org/10.1016/j.jelekin.2015.07.011>.
45. Riener, R., M. Rabuffetti, and C. Frigo, "Stair ascent and descent at different inclinations," *Gait Posture*, Vol. 15, pp. 32–44, Feb 2002. [https://doi.org/10.1016/s0966-6362\(01\)00162-x](https://doi.org/10.1016/s0966-6362(01)00162-x).
46. Riener, R., M. Rabuffetti, and C. Frigo, "Joint powers in stair climbing at different slopes," *1999 IEEE Engineering in Medicine and Biology 21st Annual Conference and the 1999 Annual Fall Meeting of the Biomedical Engineering Society (Cat. No.99CH37015, 1999)*. <https://doi.org/10.1109/iembs.1999.802608>.
47. Chang, B. C., M. I. Khan, A. Prado, *et al.*, "Biomechanical differences during ascent on regular stairs and on a stairmill, journal =",
48. Hussain, T., N. Iqbal, H. F. Maqbool, *et al.*, "Intent based recognition of walking and ramp activities for amputee using sEMG based lower limb prostheses," *Biocybernetics and Biomedical Engineering*, Vol. 40, no. 3, pp. 1110–1123, 2020. <https://doi.org/10.1016/j.bbe.2020.05.010>.
49. Eilenberg, M. F., H. Geyer, and H. Herr, "Control of a powered ankle-foot prosthesis based on a neuromuscular model," *IEEE Transactions on Neural Systems and Rehabilitation Engineering*, Vol. 18, pp. 164–173, Apr 2010. <https://doi.org/10.1109/tnsre.2009.2039620>.
50. Wu, A. R., F. Dzeladini, T. J. Brug, *et al.*, "An adaptive neuromuscular controller for assistive lower-limb exoskeletons: A preliminary study on subjects with spinal cord injury," *Frontiers in Neurobotics*, Vol. 11, Jun 2017. <https://doi.org/10.3389/fnbot.2017.00030>.
51. Goulermas, J. Y., D. Howard, C. J. Nester, *et al.*, "Regression techniques for the prediction of lower limb kinematics," *Journal of Biomechanical Engineering*, Vol. 127, pp. 1020–1024, Nov 2005. doi: 10.1115/1.2049328.
52. Zhang, L., Z. Li, Y. Hu, *et al.*, "Ankle joint torque estimation using an EMG-driven neuromusculoskeletal model and an artificial neural network model," *IEEE Transactions on Automation Science and Engineering*, Vol. 18, pp. 564–573, Apr 2021. <https://doi.org/10.1109/tase.2020.3033664>.

53. Xie, H., G. Li, X. Zhao, *et al.*, “Prediction of limb joint angles based on multi-source signals by GS-GRNN for exoskeleton wearer,” *Sensors*, Vol. 20, p. 1104, Feb 2020. <https://doi.org/10.3390/s20041104>.
54. Manal, K., K. Gravare-Silbernagel, and T. S. Buchanan, “A real-time EMG-driven musculoskeletal model of the ankle,” *Multibody System Dynamics*, Vol. 28, pp. 169–180, Nov 2011. <https://doi.org/10.1007/s11044-011-9285-4>.
55. Slajpah, S., R. Kamnik, and M. Munih, “Kinematics based sensory fusion for wearable motion assessment in human walking,” *Computer Methods and Programs in Biomedicine*, Vol. 116, pp. 131–144, Sep 2014. <https://doi.org/10.1016/j.cmpb.2013.11.012>.
56. Au, S. K., P. Bonato, and H. Herr, “An EMG-position controlled system for an active ankle-foot prosthesis: An initial experimental study,” *9th International Conference on Rehabilitation Robotics, 2005 ICORR*, pp. 375–379, 2005. <https://doi.org/10.1109/icorr.2005.1501123>.
57. Zhu, A., H. Shen, Z. Shen, *et al.*, “Prediction of human dynamic ankle moment based on surface electromyography signals,” *2019 16th International Conference on Ubiquitous Robots (UR)*, pp. 755–759, 2019. <https://doi.org/10.1109/urui.2019.8768692>.
58. Huihui, C., G. Farong, C. Chao, *et al.*, “Estimation of ankle angle based on multi-feature fusion with random forest,” *2018 37th Chinese Control Conference (CCC)*, pp. 5549–5553, 2018. <https://doi.org/10.23919/chicc.2018.8482982>.
59. Zhang, B., S. Wang, M. Zhou, *et al.*, “An adaptive framework of real-time continuous gait phase variable estimation for lower-limb wearable robots,” *Robotics and Autonomous Systems*, Vol. 143, p. 103842, 2021. <https://doi.org/10.1016/j.robot.2021.103842>.
60. Weigand, F., J. Zeiss, M. Grimmer, *et al.*, “A novel approach for gait phase estimation for different locomotion modes using kinematic shank information,” *IFAC-PapersOnLine*, Vol. 53, no. 2, pp. 8697–8703, 2020. <https://doi.org/10.1016/j.ifacol.2020.12.287>.
61. Bishe, S. S., T. Nguyen, Y. Fang, *et al.*, “Adaptive ankle exoskeleton control: Validation across diverse walking conditions,” *IEEE Transactions on Medical Robotics and Bionics*, Vol. 3, no. 3, pp. 801–812, 2021. <https://doi.org/10.1109/tmr.2021.3091519>.
62. Gupta, R., I. S. Dhindsa, and R. Agarwal, “Continuous angular position estimation of human ankle during unconstrained locomotion,” *Biomedical Signal Processing and Control*, Vol. 60, p. 101968, 2020. <https://doi.org/10.1016/j.bspc.2020.101968>.
63. Keles, A. D., and C. A. Yucesoy, “Development of a neural network based control algorithm for powered ankle prosthesis,” *Journal of Biomechanics*, Vol. 113, p. 110087, Dec 2020. <https://doi.org/10.1016/j.jbiomech.2020.110087>.
64. Su, C., S. Chen, H. Jiang, *et al.*, “Ankle joint torque prediction based on surface electromyographic and angular velocity signals,” *IEEE Access*, Vol. 8, pp. 217681–217687, 2020. <https://doi.org/10.1109/access.2020.3040820>.
65. Cosentino, S., R. Kasai, Z. Gu, *et al.*, “Knee extensor muscular activity estimation during different walking patterns: flat normal and brisk walking, stair climbing,” *2018 40th Annual International Conference of the IEEE Engineering in Medicine and Biology Society (EMBC)*, pp. 1554–1557, 2018. <https://doi.org/10.1109/embc.2018.8512518>.

66. Tam, W. K., T. Wu, Q. Zhao, *et al.*, “Human motor decoding from neural signals: a review,” *BMC Biomedical Engineering*, Vol. 1, no. 22, 2019. <https://bmcbiomedeng.biomedcentral.com/articles/10.1186/s42490-019-0022-z>.
67. Stegeman, D. F., and H. J. Hermens, “Proceedings of the third general SENIAM workshop on surface electromyography,” in *In: Hermens H.J., Rau G., Disselhorst-Klug C., Freriks B. (Eds.), Surface Electromyography Application Areas and Parameters. Proceedings of the Third General SENIAM Workshop on surface electromyography*, (Aachen-Germany), pp. 108–112, 1998.
68. Luca, C. J. D., L. D. Gilmore, M. Kuznetsov, *et al.*, “Filtering the surface EMG signal: Movement artifact and baseline noise contamination,” *Journal of Biomechanics*, Vol. 43, pp. 1573–1579, May 2010. <https://doi.org/10.1016/j.jbiomech.2010.01.027>.
69. Merletti, R., A. Rainoldi, and D. Farina, “Surface electromyography for noninvasive characterization of muscle,” *Exercise and Sport Sciences Reviews*, Vol. 29, pp. 20–25, Jan 2001. <https://doi.org/10.1097/00003677-200101000-00005>.
70. Smith, L. H., L. J. Hargrove, B. A. Lock, *et al.*, “Determining the optimal window length for pattern recognition-based myoelectric control: Balancing the competing effects of classification error and controller delay,” *IEEE Transactions on Neural Systems and Rehabilitation Engineering*, Vol. 19, pp. 186–192, Apr 2011. <https://doi.org/10.1109/tnsre.2010.2100828>.
71. Du, S., and M. I. Vuskovic, “Temporal vs. spectral approach to feature extraction from prehensile EMG signals,” *Proc. IEEE Int. Conf. Inf. Reuse Integration*, pp. 344–350, Nov 2004.
72. Englehart, K., B. Hudgins, and P. A. Parker, “A wavelet-based continuous classification scheme for multifunction myoelectric control,” *IEEE Transactions on Biomedical Engineering*, Vol. 48, pp. 302–311, Mar 2001.
73. Farrell, F. R., and R. F. Weir, “The optimal controller delay for myoelectric prostheses,” *IEEE Transactions on Neural Systems and Rehabilitation Engineering*, Vol. 15, pp. 111–118, Mar 2007. <https://doi.org/10.1109/tnsre.2007.891391>.
74. Zarshenas, H., B. P. Ruddy, A. W. Kempa-Liehr, *et al.*, “Ankle torque forecasting using time-delayed neural networks,” *2020 42nd Annual International Conference of the IEEE Engineering in Medicine & Biology Society (EMBC)*, pp. 4854–4857, 2020. <https://doi.org/10.1109/embc44109.2020.9175376>.
75. Xu, K., W. Guo, L. Hua, *et al.*, “A prosthetic arm based on EMG pattern recognition,” *2016 IEEE International Conference on Robotics and Biomimetics (ROBIO)*, pp. 1179–1184, 2016. <https://doi.org/10.1109/robio.2016.7866485>.
76. Englehart, K., and B. Hudgins, “A robust, real-time control scheme for multifunction myoelectric control,” *IEEE Transactions on Biomedical Engineering*, Vol. 50, no. 7, pp. 848–854, 2003. <https://doi.org/10.1109/tbme.2003.813539>.
77. Dehghani, A., O. Sarbishei, T. Glatard, *et al.*, “A quantitative comparison of overlapping and non-overlapping sliding windows for human activity recognition using inertial sensors,” *Sensors*, Vol. 19, no. 22, p. 5026, 2019. <https://doi.org/10.3390/s19225026>.

78. Cui, C., G. B. Bian, Z. G. Hou, *et al.*, “sEMG-based prediction of human lower extremity movements by using a dynamic recurrent neural network,” *2016 Chinese Control and Decision Conference (CCDC)*, pp. 5021–5026, 2016. <https://doi.org/10.1109/ccdc.2016.7531892>.
79. Chowdhury, R., M. Reaz, M. Ali, *et al.*, “Surface electromyography signal processing and classification techniques,” *Sensors*, Vol. 13, no. 9, pp. 12431–12466, 2013. <https://doi.org/10.3390/s130912431>.
80. Ibrahimy, M. I., O. O. Khalifa, and M. R. Ahsan, “EMG motion pattern classification through design and optimization of neural network,” *Proceedings of the International Conference on Biomedical Engineering (ICoBE)*, Feb 2012.
81. Asghari, M. O., and H. Hu, “Myoelectric control systems-a survey,” *Biomedical Signal Processing and Control*, Vol. 2, pp. 275–294, Oct 2007. <https://doi.org/10.1016/j.bspc.2007.07.009>.
82. Holm, S., and P. K. Eide, “The frequency domain versus time domain methods for processing of intracranial pressure (ICP) signals,” *Medical Engineering Physics*, Vol. 30, no. 2, pp. 164–170, 2008. <https://doi.org/10.1016/j.medengphy.2007.03.003>.
83. Hudgins, B., P. Parker, and R. N. Scott, “A new strategy for multifunction myoelectric control,” *IEEE Transactions on Biomedical Engineering*, Vol. 40, no. 1, pp. 82–94, 1993. <https://doi.org/10.1109/10.204774>.
84. Phinyomark, A. N., R. Khusbaba, and E. Scheme, “Feature extraction and selection for myoelectric control based on wearable EMG sensors,” *Sensors*, Vol. 18, no. 5, p. 1615, 2018. <https://doi.org/10.3390/s18051615>.
85. Tang, G., J. Sheng, D. Wang, *et al.*, “Continuous estimation of human upper limb joint angles by using PSO-LSTM model,” *IEEE Access*, Vol. 9, pp. 17986–17997, 2021. <https://doi.org/10.1109/access.2020.3047828>.
86. Hargrove, L. J., G. Li, K. B. Englehart, *et al.*, “Principal components analysis preprocessing for improved classification accuracies in pattern-recognition-based myoelectric control,” *IEEE Transactions on Biomedical Engineering*, Vol. 56, no. 5, pp. 1407–1414, 2009. <https://doi.org/10.1109/tbme.2008.2008171>.
87. Tkach, D., H. Huang, and T. A. Kuiken, “Study of stability of time-domain features for electromyographic pattern recognition,” *Journal of NeuroEngineering and Rehabilitation*, Vol. 7, May 2010. <https://doi.org/10.1186/1743-0003-7-21>.
88. Phinyomark, A., C. Limsakul, and P. Phukpattaranont, “EMG feature extraction for tolerance of white gaussian noise,” *International Workshop and Symposium Science Technology (I-SEEC 2008)At: Nong Khai, Thailand*, Dec 2008.
89. Mohamed, H. S., G. E. Mohamed, D. M. Mosaad, *et al.*, “Effect of ischaemic compression versus kinesiotape on patellar tendinitis,” *Physiotherapy Quarterly*, Vol. 29, no. 1, pp. 47–55, 2021. <https://doi.org/10.5114/pq.2020.96425>.
90. Ajiboye, A. B., and R. F. Weir, “A heuristic fuzzy logic approach to EMG pattern recognition for multifunctional prosthesis control,” *IEEE Transactions on Neural Systems and Rehabilitation Engineering*, Vol. 13, no. 3, pp. 280–291, 2005.
91. Kaiser, M., “Time-delay neural networks for control,” *IFAC Proceedings Volumes*, Vol. 27, no. 14, pp. 967–972, 1994. [https://doi.org/10.1016/s1474-6670\(17\)47423-4](https://doi.org/10.1016/s1474-6670(17)47423-4).

92. Kayri, M., “Predictive abilities of Bayesian regularization and Levenberg-Marquardt algorithms in artificial neural networks: A comparative empirical study on social data,” *Mathematical and Computational Applications*, Vol. 21, no. 2, p. 20, 2016. <https://doi.org/10.3390/mca21020020>.
93. Marwala, T., “Bayesian training of neural networks using genetic programming,” *Pattern Recognition Letters*, Vol. 28, no. 12, pp. 1452–1458, 2007. <https://doi.org/10.1016/j.patrec.2007.03.004>.
94. Yi, C., F. Jiang, S. Zhang, *et al.*, “Continuous prediction of lower-limb kinematics from multi-modal biomedical signals,” *IEEE Transactions on Circuits and Systems for Video Technology*.
95. Kaushik, S., A. Choudhury, P. K. Sheron, *et al.*, “AI in healthcare: Time-series forecasting using statistical, neural, and ensemble architectures,” *Frontiers in Big Data*, Vol. 3, 2020. <https://doi.org/10.3389/fdata.2020.00004>.
96. Francisco, M., S. Revollar, P. Vega, *et al.*, “A comparative study of deterministic and stochastic optimization methods for integrated design of processes,” *IFAC Proceedings Volumes*, Vol. 38, no. 1, pp. 335–340, 2005. <https://doi.org/10.3182/20050703-6-cz-1902.00917>.
97. Kingma, D. P., and J. Ba, “Adam: A method for stochastic optimization,” 2014. arXiv preprint arXiv:1412.6980.
98. Liashchynskiy, P., “Grid search, random search, genetic algorithm: a big comparison for NAS,” 2019. arXiv preprint arXiv:1912.06059.
99. Mori, N., M. Takeda, and K. Matsumoto, “A statistical comparison study between genetic algorithms and Bayesian optimization algorithms,” *Progress of Theoretical Physics Supplement*, Vol. 157, pp. 353–356, 2005. <https://doi.org/10.1143/ptps.157.353>.
100. Saeb, S., L. Lonini, A. Jayaraman, *et al.*, “The need to approximate the use-case in clinical machine learning,” *GigaScience*, Vol. 6, no. 5, 2017. <https://doi.org/10.1093/gigascience/gix019>.
101. Little, M. A., G. Varoquaux, S. Saeb, *et al.*, “Using and understanding cross-validation strategies. perspectives on Saeb et al.,” *GigaScience*, Vol. 6, no. 5, 2017. <https://doi.org/10.1093/gigascience/gix020>.
102. Raschka, S., “Model evaluation, model selection, and algorithm selection in machine learning,” 2018. arXiv preprint arXiv:1811.12808.
103. Bogey, R. A., and L. A. Barnes, “An EMG-to-force processing approach for estimating in vivo hip muscle forces in normal human walking,” *IEEE Transactions on Neural Systems and Rehabilitation Engineering*, Vol. 25, pp. 1172–1179, Aug 2017. <https://doi.org/10.1109/tnsre.2016.2613021>.
104. Dhir, N., H. Dallali, E. M. Ficanha, *et al.*, “Locomotion envelopes for adaptive control of powered ankle prostheses,” *2018 IEEE International Conference on Robotics and Automation (ICRA)*, pp. 1488–1495, 2018. <https://doi.org/10.1109/icra.2018.8460929>.
105. Prasertsakul, T., J. Poonsiri, and W. Charoensuk, “Prediction gait during ascending stair by using artificial neural networks,” *The 5th 2012 Biomedical Engineering International Conference*, pp. 1–5, 2012. <https://doi.org/10.1109/bmeicon.2012.6465464>.

106. Schwartz, M. H., A. Rozumalski, and J. P. Trost, “The effect of walking speed on the gait of typically developing children,” *Journal of Biomechanics*, Vol. 41, no. 8, pp. 1639–1650, 2008. <https://doi.org/10.1016/j.jbiomech.2008.03.015>.
107. Bovi, G., M. Rabuffetti, P. Mazzoleni, *et al.*, “A multiple-task gait analysis approach: kinematic, kinetic and EMG reference data for healthy young and adult subjects,” *Gait & Posture*, Vol. 33, no. 1, pp. 6–13, 2011. <https://doi.org/10.1016/j.gaitpost.2010.08.009>.
108. Horst, F., S. Lapuschkin, W. Samek, *et al.*, “Explaining the unique nature of individual gait patterns with deep learning,” *Scientific Reports*, Vol. 9, no. 1, pp. 11–13, 2019. <https://doi.org/10.17632/svx74xcrjr.3>.
109. Hoover, C. D., G. D. Fulk, and K. B. Fite, “Stair ascent with a powered transfemoral prosthesis under direct myoelectric control,” *IEEE/ASME Transactions on Mechatronics*, Vol. 18, no. 3, pp. 1191–1200, 2013. <https://doi.org/10.1109/tmech.2012.2200498>.